2014

TEST-ANALYSIS MODEL CORRELATION AND CALIBRATION OF A MULTI-COMPONENT PLASTIC PART

Steven P. Carter
Michigan Technological University

TEST-ANALYSIS MODEL CORRELATION AND CALIBRATION OF A MULTI-COMPONENT PLASTIC PART

By

Steven P. Carter

A THESIS

Submitted in partial fulfillment of the requirements for the degree of

MASTER OF SCIENCE

In Mechanical Engineering

MICHIGAN TECHNOLOGICAL UNIVERSITY

2014

This thesis has been approved in partial fulfillment of the requirements for the Degree of MASTER OF SCIENCE in Mechanical Engineering.

Department of Mechanical Engineering-Engineering Mechanics

Thesis Advisor: *Charles D. Van Karsen*

Committee Member: *James DeClerck*

Committee Member: *Allan A, Struthers*

Department Chair: *William W. Predebon*

Acknowledgements

It's hard to know where to begin my acknowledgements; there are so many people who helped me get to this point in my so-called academic career. I suppose it would be most fitting to start with my advisor, Chuck Van Karsen. Without him I would have been lost in this project, his advice and guidance was invaluable and continues to make a difference in my work today. I also owe a debt of gratitude to the other professors who opened my eyes to the beautiful world of sound and vibration: Dr. Mohan Rao, Dr. James DeClerck, and Dr. Jason Blough.

I would also like to thank Jamie, Surdi, Mike, Wally, and Andy. You all helped to drag me through the pain of graduate school coursework. There were so many times I was ready to stop before the job was done, but you gave me the motivation to continue. Last but not least, I should thank my parents. It was the effort you put into my upbringing that allowed me to reach this point.

I also want to thank anyone who's reading this thesis, you're making the effort I put into writing it worthwhile.

Table of Contents

Abstract

The goal of this project is to learn the necessary steps to create a finite element model, which can accurately predict the dynamic response of a Kohler Engines Heavy Duty Air Cleaner (HDAC). This air cleaner is composed of three glass reinforced plastic components and two air filters. Several uncertainties arose in the finite element (FE) model due to the HDAC's component material properties and assembly conditions. To help understand and mitigate these uncertainties, analytical and experimental modal models were created concurrently to perform a model correlation and calibration. Over the course of the project simple and practical methods were found for future FE model creation. Similarly, an experimental method for the optimal acquisition of experimental modal data was arrived upon. After the model correlation and calibration was performed a validation experiment was used to confirm the FE models predictive capabilities.

Chapter 1: Introduction

Finite element (FE) models have become very powerful tools for product development. A quality FE model can help reduce the need for physical prototyping and testing, which in turn can reduce time and costs involved with the design process. This is because a model can be used in an iterative method to find and test engineered solutions where it would be infeasible, or time/cost prohibitive to do so with a physical prototype. Examples of this are in large-scale projects such as up or down gauging the steel in a vehicles frame and body panels, or in situations where expensive tooling would be required such as molded plastic parts.

For effective use, an FE model must match the physical system it is intended to represent. As such, the FE model should predict any desired characteristics such as durability, strength, dynamic response, etc. These capabilities are typically verified through model correlation and validation. This is a process that compares the FE models computed results to those found through physical tests. Common methods used for the comparison of modal models (as is done in this thesis) are described in section 2.1 below. In addition to correlation and validation, FE models can also be calibrated. This is the process of adjusting various parameters (e.g. material properties, joint stiffness's, part geometry, etc.) in an effort to improve the FE models accuracy.

1.1 Objectives

This project takes a first look at the methods needed to create a correlated FE model of a Kohler Engines Heavy Duty Air Cleaner (HDAC). The fundamental goal of this correlation was to be able to accurately predict the systems dynamic response to a broadband random input. For the purposes of this thesis, an accurately predicted response

will have an overall level that is within three decibels of the measured response and a spectrum that depicts the same general shape as the measured spectrum (judged through subjective analysis). This goal was accomplished through the completion of six steps:

1. FE models were created to predict the mode shapes and natural frequencies of each of the HDAC's structural components (referred to as analytical modal models). Damping was omitted from the FE model during this step of the project. These FE models were constructed keeping efficiency and simplicity in mind. To this end, the original CAD geometry was modified to remove geometrical features, which were deemed unnecessary to the analytical modal models calculation. The allowable level of these simplifications was determined through a trial and error process that was checked during step three (model correlation).
2. In conjunction with step one, experimental modal models were created for each of the HDAC's structural components. A test method was developed for this to provide consistent results with minimal experimental error for modal parameter estimation. This test method was designed to avoid common experimental errors such as mass loading, non-linear effects, and hard to estimate boundary conditions. Similar to the FE models creation, this test method was developed through a trial and error process that was checked in step three (model correlation).
3. After developing the modal models in steps one and two, they were compared with one another using common model correlation techniques (i.e. global mass comparison, modal assurance criterion, and natural frequency difference). The results of these correlations were then analyzed to determine if the modal models could be deemed accurate based on their similarity (if they represent the same dynamic system). If this was not the case, then possible sources of error were hypothesized

(e.g. FE model oversimplification, incorrect experimental modal parameter estimation, etc.) and steps one and two were revisited to address possible errors.

4. Once the modal models were deemed accurate, the FE model was calibrated to better match the experimental model. This was accomplished by adjusting geometrical and material properties. Model calibration was performed so the FE model could better match the physical system (assuming that the experimental model is correct and representative).
5. After steps one through four were completed for the individual HDAC components, they were repeated for the assembled system. To accomplish this, the HDACs individual component FE models were configured to represent the physical system, while the experimental data was collected on the assembled system. At this step the only sources of error that were addressed were due to the HDACs assembly conditions. This is because the significant errors in the individual component models had already been quantified and addressed where possible.
6. The final step in this project was to perform a model validation experiment to confirm or deny the FE models accuracy. This experiment consisted of providing a known broadband random input and measuring/computing the response at three locations, one per plastic component. The resulting responses at these locations were then compared to make conclusions on the FE models predictive capabilities. It is important to note that the computed response was a blind prediction. This means that neither the FE model or response measurement technique was adjusted to increase the favorability of the response comparisons. If any errors were found they were to be addressed through the re-visitation of steps one through five.

As George Box put it "Essentially, all models are wrong, but some are useful" this project attempts to make an FE model, which is useful to predict the HDAC's dynamic response.

1.2 Kohler Engines Heavy Duty Air Cleaner

The HDAC is comprised of five primary components; these can be seen in Figure 1.1 below. The assembled HDAC is shown in Figure 1.2. Table 1.1 shows pictures of the parts along with a short description of the part and its function. The clip that connects the plastic parts is not considered a primary component. As such is not shown below and was not individually tested or modeled. It was hypothesized that this clip only affected the assembly's connections (minimal added mass and modal properties) and could be simulated in the FE model using connection elements.

Throughout this thesis certain sections of the plastic components will be referred to as the top or the shell. The top of the end caps refers to the closed end of the part with the Kohler logo on it. The term shell refers to the cylindrical portions of the all the plastic parts.

Figure 1.1: The five primary components of the heavy-duty air cleaner

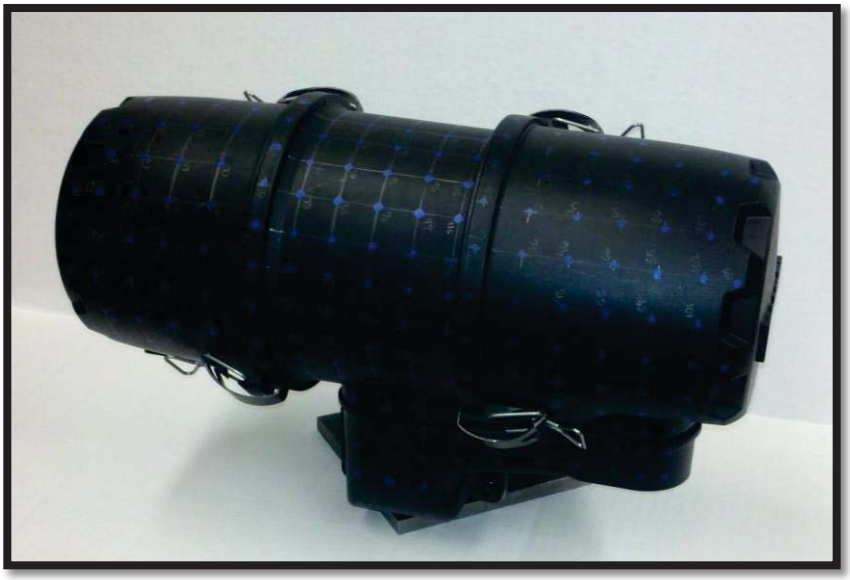

Figure 1.2: The assembled heavy-duty air cleaner

Table 1.1: The primary components of the HDAC with part numbers and descriptions

Picture	Part Number	Description
	6209401 (referred to as center section)	This is the piece of the air cleaner which houses the air filters and connects to an engines intake manifold. This part is actually comprised of two pieces, one part that connects to manifold and the other that houses the air filters. These two are permanently welded together and as such will be referred to as one part.
	6209622 (referred to as open end cap)	This is the end cap, which attaches to the open side of part no. 6209401. It helps to house and locate the air filters.
	6209625 (referred to as closed end cap)	This is the end cap, which attaches to the closed end of 6209401. It covers the main air intake portion of the HDAC. As such, its main purpose is to help protect the air inlet from the elements.
	2508301 (referred to as outer filter)	This is one of the two air filters in the system. It is the larger of the two air filters. It is loosely press fit by hand into part no. 6209401
	258304 (referred to as inner filter)	This is the smaller of the systems two air filters. It fits inside of part no. 2508301 and is loosely press fit by hand into part no. 6209401.

Chapter 2: Literature Review

This chapter will provide an overview of the research that was done to create the rough framework for this thesis project. It is broken up into three sections, the first will cover commonly available model correlation techniques as well as their advantages and disadvantages, the second will discuss modal testing considerations which could affect the correlations success, the final section will discuss the ability to predict material properties and model parameters through model correlation.

2.1 Model Correlation Techniques

There are several methods available to perform a model correlation using modal parameters. A survey by Hasselman et al[1] outlined the most commonly used methods; these are: percent frequency difference (Equation 2.1), modal pseudo-orthogonality Avitabile et al[2] (Equation 2.2), and the modal assurance criterion (MAC) Allemang[3] (Equation 2.3).

$$\Sigma_{frequncy\,r} = \frac{|f_{tr} - f_{ar}|}{f_{tr}} 100 \qquad \text{Equation 2.1}$$

$$[\Phi_a]^T[M][\Phi_t] = [M_{modal}] \approx [I] \qquad \text{Equation 2.2}$$

$$MAC_{tvr} = \frac{|\{\Psi_{tr}\}^H\{\Psi_{vr}\}|^2}{(\{\Psi_{tr}\}^H\{\Psi_{tr}\})(\{\Psi_{vr}\}^H\{\Psi_{vr}\})} \qquad \text{Equation 2.3}$$

where:

f_{tr} = The rth test natural frequency

f_{ar} = The rth analytical natural frequency

Φ_a = The mode shape matrix found from the analytical modal analysis

Φ_t = The mode shape matrix found from the test data

M = The systems mass matrix

Ψ_{vr} = The rth mode shape vector of the model to be validated (the finite element model)

Ψ_{tr} = The rth mode shape vector found from the test data

The natural frequency error check is a simple calculation, which determines percent error between the two different natural frequency estimates (from the analytical and experimental models). The goal of this comparison is to have a frequency difference that is as low as possible. An error of %10 is typically considered acceptable, although this may change depending on accuracy requirements. The acceptable error should take the part to part and test variability into account.

Modal pseudo-orthogonality is a check, which determines if two different mode shape matrices were found from models (analytical or experimental) that represent the same dynamic system. This is accomplished through a matrix computation, which maps the systems mass or stiffness matrices into modal space. This is useful because the modal mass and stiffness matrices are theoretically known. Most often the systems mass matrix is used because it will ideally result in an identity matrix (depending on modal vector scaling), making the results easier to analyze.

This modal pseudo-orthogonality check provides a very strong indication of modal model similarity. But, is disadvantageous in that the experimental and analytical models need to have the same number of degrees of freedom. To accomplish this the either the experimental modal model be expanded or (more typically) that analytical model be reduced. This is referred to as the development of the test-analysis model (TAM) Flanigan[5].

Reducing the analytical modal matrices can simply be done through eliminating the desired DOFs, but reducing the system (mass and stiffness) matrices requires more complex techniques. This is because the reduced system matrices should preserve both the local and global system properties. The most commonly used method for this is the Guyan[6] reduction,

also known as static condensation. However, care must be taken when using this method, as the inertia of the eliminated degrees of freedom is lost.

This will inevitably lead to inaccuracies depending on the locations of the preserved DOFs. As such, care should be taken to ensure that the preserved DOFs will account for the majority of the systems mass. If this is not done, the reduction will lead to an incorrect mass matrix, which in turn results in false orthogonality check. O'Callahan et al[7] outlined a reduction method (called SEREP) to overcome these errors. The reduced mass matrix found using this method preserves the dynamics of the system exactly. While this method has several advantages, it is less established and not commonly available in commercial software.

The modal assurance criterion is a correlation coefficient, which is used to "provide a measure of consistency (degree of linearity) between estimates of a modal vector" (Allemang[3]). MAC provides a significant advantage when compared to modal pseudo-orthogonality, as it does not require reduced system matrices. Because of this, MAC is more commonly used then pseudo-orthogonality even though it doesn't provide as strong of an indicator of model similarity.

The MAC calculation results in values ranging from zero to one, representing either a very weak or strong correlation respectively. It is important to note that MAC is only a correlation coefficient and does not indicate validity or orthogonality. This can lead situations where the MAC value results in false indications of correlation or non-correlation. Falsely low MAC values generally are the result of "noisy" modal vectors or system nonlinearities. Falsely high MAC values are most often caused by spatial aliasing where two different modal vectors look similar. Because of this, the modal assurance criterion should be used with care.

In addition to the above methods it is also suggested that the FE models global mass be compared to the experimental systems global mass Heylen et al[4]. This is often the first step during a model correlation because it is extremely simple and straightforward. Using this comparison an initial validation or rejection of the analytical mass matrix can be made.

2.2 Modal Testing Considerations

There are several topics concerning the modal test to ensure high quality results. It is important that these be addressed, as any errors in the experimental data will reduce the model correlations accuracy. By paying attention to the considerations listed below during the modal test, errors in the correlation can be minimized or at least accounted for.

A paper by Avitabile[8] discusses most of the common testing considerations, which can affect the success of the correlation. This paper breaks down these considerations into six groups: overall system level concerns, test set-up, signal processing, excitation methods, modal parameter estimation, and pre-test concerns.

The overall system level concerns mainly relate to the systems consistency; and are time invariance, linearity, reciprocity, and repeatability. These factors address how consistently the modal parameters can be estimated, based on how, where, and when the system is analyzed. An ideal system for the modal testing would be completely time invariant, linear, reciprocal, and repeatable. This is rarely the case however and because of this modal tests are performed in a quasi-static state; where the system level concerns can be accounted for and understood.

The test set-up considerations are concerned with ensuring that the same system is being analyzed in both the FE model and modal test. Things such as the test boundary and the effects of the instrumentation (locally added mass and stiffness) must be considered.

These effects must either be minimized in test or accounted for in the FE model. If this is not done then the correlation will yield poor results because the analytical and experimental models will be based on different systems.

The signal processing considerations have concerns related to measurement distortion. This is caused be the fact that the measurements are a discrete approximation of the actual systems response. Typically, these concerns are easily mitigated using modern data acquisition techniques in a lab environment modal test, but they still should be considered to avoid any possible problems.

The effects of the excitation technique on the resulting data should be considered when collecting the modal data. There are two main concerns when considering the excitation technique: run-to-run repeatability, and how the excitation will affect system non-linearity's. If these concerns are not addressed the results of the modal test could contain significant errors.

Finally, the measurement locations must be chosen so that the desired mode shapes are well defined. Typically this is done based on experience and intuition but in the case where a FE model of the system exists pre-test analysis can be performed to determine optimal test points. When doing this it is important to realize that the FE model may not be predicting the actual structures dynamics. As such, care must be taken in order to avoid choosing an inadequate set of test points. In some cases it may be necessary to revisit the modal test and refine the measurement locations.

2.3 Model Parameter Estimation Using Model Calibration

Results published by Blaschke et al[9] and Veers et al[10] show the application of model correlation and calibration to determine material properties for plastic and composite

materials, respectively. These papers show that a simple model correlation and calibration method based on standard test and analysis methods can be used to determine uncertain or unknown material properties. This is the approach that was taken to help determine or verify the HDAC's material properties.

Chapter 3: Theory and Analysis Methods

This chapter will introduce the theoretical modal model as well as the methods used to assess the FE models usefulness. The theoretical modal model shown below is used to understand a systems dynamics both analytically and experimentally. Along with a discussion of the theory, this chapter will also describe the approaches taken to perform the modal analyses, model correlation, and model calibration. It should also be noted that the content below is only a brief overview the methods used. For a more complete set of descriptions and derivations Modal Analysis Testing and Theory[4] is suggested.

3.1 Theoretical Modal Model

Almost all of the work in this thesis has its basis in the modal model described below. As such, an understanding of this model and its properties is critical. The first step in a dynamic analysis is to formulate the systems equations of motion; this is shown in Equation 3.1 below.

$$[M]_{NxN}\{\ddot{x}\}_{Nx1} + [C]_{NxN}\{\dot{x}\}_{Nx1} + [K]_{NxN}\{x\}_{Nx1} = \{F\}_{Nx1} \qquad \text{Equation 3.1}$$

where:

N = The number of dof's in the system

$[M]$ = The mass matrix

$[C]$ = The damping matrix

$[K]$ = The stiffness matrix

$\{\ddot{x}\}$, $\{\dot{x}\}$, and $\{x\}$ = The second, first, and zeroth derivative of the system displacements

$\{F\}$ = The external forces acting on the system

To determine a systems modal parameters, the external forces are set to zero and the equations of motion are converted into the Laplace domain, this is shown in Equation 3.2.

$$(s^2[M] + s[C] + [K])\{X\} = 0 \qquad \text{Equation 3.2}$$

If general viscous damping is assumed, then solving the eigenvalue problem corresponding to Equation 3.2 can be done to find the systems poles (Equation 3.3) and complex valued mode shapes. Typically, FE models assume either zero or proportional damping; with zero damping, Equation 3.2 can be simplified into Equation 3.4.

$$\lambda_r = -\zeta_r\omega_r + j\omega_r\sqrt{1-\zeta_r^2} \qquad \text{Equation 3.3}$$

where:

λ_r = The rth pole of the FRF

ω_r = The rth natural frequency of the system

ζ_r = The damping ratio for the rth natural frequency of the system

$$(s^2[M] + [K])\{X\} = 0 \qquad \text{Equation 3.4}$$

Solving the generalized eigenvalue problem related to Equation 3.4 results in N real valued eigenvalues (natural frequencies squared) and N real valued eigenvectors (mode shapes). If the system is proportionally damped then the systems mode shapes will be the same, except with a different scaling.

The system can also be described by its transfer function, shown in Equation 3.5. This is done by inverting the systems characteristic equation, equation 3.2 where the forces are not set to zero.

$$H(s) = \frac{X(s)}{F(s)} = \left[[M]s^2 + [C]s + [K]\right]^{-1} \qquad \text{Equation 3.5}$$

The systems transfer function describes how it will react to any input. If this is evaluated along the frequency axis ($s = j\omega$), it is called the frequency response function (FRF), shown in Equation 3.6.

$$H(j\omega) = \frac{X(j\omega)}{F(j\omega)} = \left[-\omega^2[M] + j\omega[C] + [K]\right]^{-1} \quad \text{Equation 3.6}$$

The systems FRF can also be formulated using its modal parameters in what is called pole-residue format. This is shown below in Equation 3.7. The pole-residue FRF format is most often used during experimental modal parameter estimation.

$$H(j\omega) = \sum_{r=1}^{N} \left(\frac{Q_r \{\Psi\}_r \{\Psi\}_r^T}{(j\omega - \lambda_r)} + \frac{Q_r^* \{\Psi\}_r^* \{\Psi\}_r^{*T}}{(j\omega - \lambda_r^*)} \right) \quad \text{Equation 3.7}$$

where:

Ψ_r = The rth mode shape vector of the FRF

Q_r = The rth mode shape scaling factor, which is dependent on each mode

N = The number of modes in the system

3.2 Analytical Modal Analysis Approach

An analytical modal analysis uses either Equation 3.2 or 3.4 to calculate a system's modal parameters based upon estimates of its mass, stiffness, and damping matrices. This implies that this analysis' quality is dependent on the accuracy of the system matrices estimates. Because of this, the main focus of an analytical modal analysis is determining the system matrices, most often using the finite element method.

The finite element method is the process of approximating a structures geometry using discrete elements such as beams, plates, and tetrahedrons. Because the geometry of these elements is absolutely known, equations can be formulated to describe the their mass, stiffness, and damping properties. Using these elements to describe the geometry an entire

structure results in its mass, stiffness, and damping matrices. Because of the variety of available element types, the derivations are not shown here; for more information any introductory book on the finite element method is suggested.

Since the system matrices are defined by the elements geometry it is important that they are well conditioned. This is because poorly conditioned elements can cause artificial stiffening, numerical instability, etc. To avoid this, model checks are performed, which analyze the elements shape. For two-dimensional elements, common examples of these checks are aspect ratio, skew, stretch, and minimum/maximum interior angle.

3.3 Experimental Modal Analysis Approach

An experimental modal analysis estimates the modal parameters of a system using directly measured frequency response functions. This is done by providing excitation and measuring the system inputs and outputs at various locations on the structure (measurement degrees of freedom (DOF)). There are three main steps in performing an experimental modal analysis: the measurement set-up, data acquisition, and modal parameter estimation.

The measurement set-up step is where the various test parameters such as excitation technique, response transducers, measurement DOF locations, and boundary conditions are chosen. The first part of the test set-up that should be determined is the boundary conditions; typically the part will either be suspended in a free-free boundary condition or the system will be set-up as they are "in-use". After this is done the measurement locations should be chosen based on the expected mode shapes. Locations should be chosen where large amounts of motion are expected.

Finally, the excitation technique must be chosen. There are essentially two different excitation technique types, shaker type tests or impact type tests. Shaker excitation is

generally much more consistent, but requires that the instrumentation be moved to each measurement location, possibly causing increase mass loading errors. Impact excitation is less consistent and can possible excite nonlinearities, but generally has a smaller affect on the system since there is no need to move the instrumentation.

Once the measurement set-up has been chosen, the FRFs can be measured. First the bandwidth and frequency resolution must be chosen. These are based on the sampling frequency (F_S) and the number of samples to read (N). While choosing the bandwidth is fairly straightforward, picking the frequency resolution isn't necessarily as simple. A higher frequency resolution can make modal parameter estimation (described below) easier, but generally allows more noise into the FRF and adds time to the data acquisition. The equations relating sampling frequency and samples to read to frequency resolution and bandwidth are shown below in Equations 3.8 and 3.9. (Smith[11])

$$\text{Bandwidth} = {}^{F_S}/_{2} \qquad \text{Equation 3.8}$$

$$\text{Frequency Resolution} = {}^{N}/_{F_S} \qquad \text{Equation 3.9}$$

When acquiring the data it is important to verify the quality of the data. This is done by observing the systems responses, frequency response functions, and coherence. By ensuring that the measurements remain consistent, the validity of the data may be assessed.

With the data collected, the modal parameters may be estimated. This is the process where the natural frequencies, damping ratios, and mode shapes of a system are estimated using the measured FRF's. There are several different methods to do this, but most are based on assuming the modal model describe in section 3.1. These models are formulated using either a single or multiple degree of freedom system. Most often the MDOF modal

models are fitted in a least squares sense to the measured data by estimating the systems poles and residues (Equation 3.4). This can be done in either the time or frequency domain.

3.4 Model Correlation and Calibration Approach

The model correlation is performed using the natural frequency error, global mass comparison, and modal assurance criterion described in section 2.1. After any errors have been found and possibly corrected during the model correlation, the FE model is ready to be calibrated in order to improve its performance. It is important to ensure that errors in the FE models predictions aren't being caused by things like faulty element connectivity, incorrect boundary conditions, etc. (Mayes[12]) before the calibration is performed. This is because the model calibration only adjusts geometric parameters and material properties, and as such will not account for those types of errors.

The model correlation is normally performed through a gradient based optimization, where the goals of the optimization are typically to maximize MAC values and minimize frequency differences. Because of how the model is being updated, it is important that thought and care be put into the optimization set-up and calibration results analysis. This is because the model calibration will only find a solution that meets its goals and may not determine realistic model parameters.

Chapter 4: HDAC Component Modal Analysis Set-Up

This chapter discusses the set-up for the analytical and experimental modal analyses used for the components' model correlation and calibration. The test fixtures, transducer set-up, and excitation techniques will be explained for the experimental modal analyses. Similarly the modeling techniques such as the geometric simplifications and finite element mesh parameters will be described for the analytical modal analysis. The free-free boundary condition was used in each modal analysis (an approximation was used in the experimental cases). This was done in order to reduce the error when trying to model the boundary conditions and help improve the model correlation. For the data acquisition set-up parameters refer to appendix A in chapter 9.

4.1 Analytical Modal Analysis Set-Up

Finite element models were created for each of the structural components of the HDAC to perform the analytical modal analysis. The modal solution for these models was found using MSC.Nastran with the normal modes (SOL 103 – Lanczos) solution type.

4.1.1 Finite Element Model Geometric Simplifications

The finite element models were created using simplified and de-featured versions of the original 3D CAD geometry. The solid geometry was simplified into a set of surfaces, which are representative of the original system. This was done to reduce the complexity and computational cost of the FE model. For the same reasons, effort was put into simplifying the geometry into as few surfaces as possible. Doing this lowers the total amount of mesh components and thereby reduces the need to connect those mesh components, which reduces the possibility for dependency conflicts and artificial stiffening. The original CAD

geometry along with the simplified CAD geometry is shown below in Figures 4.1 through 4.6.

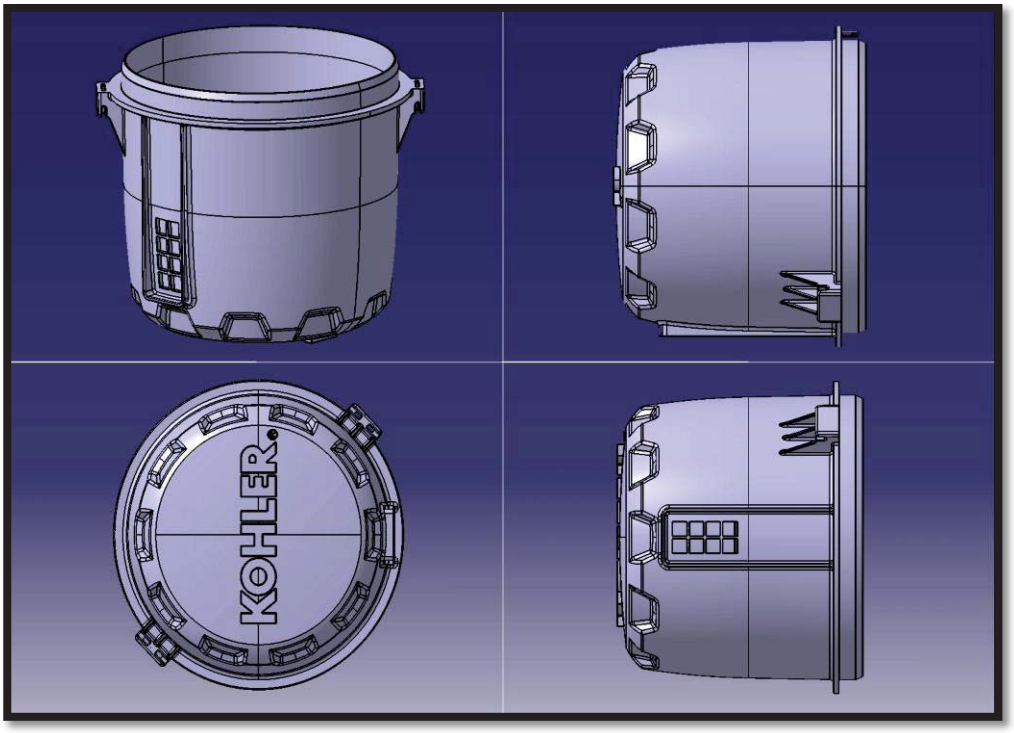

Figure 4.1: The Open End Caps original 3D CAD model

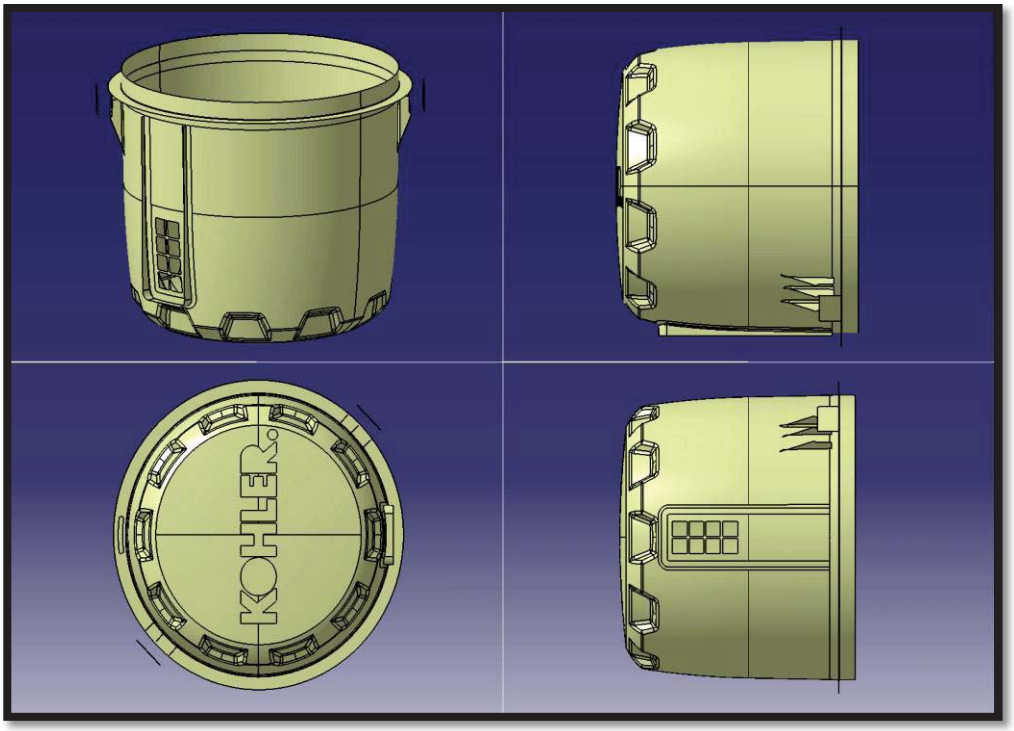

Figure 4.2: The Open End Caps simplified 3D CAD model

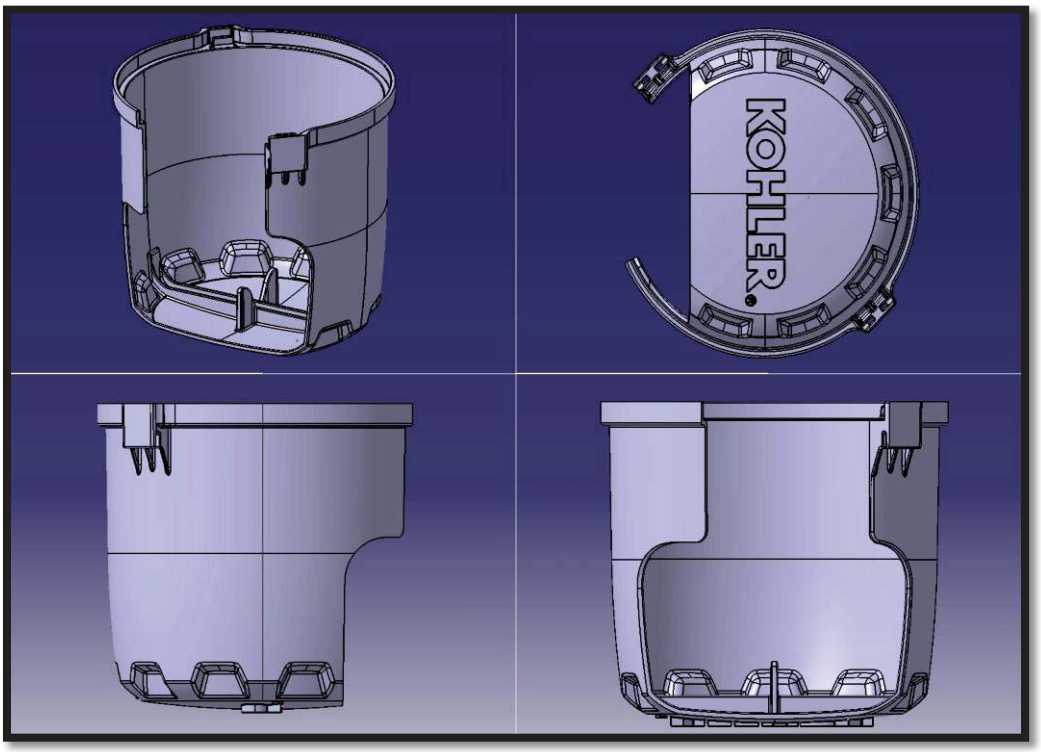

Figure 4.3: The Closed End Caps original 3D CAD model

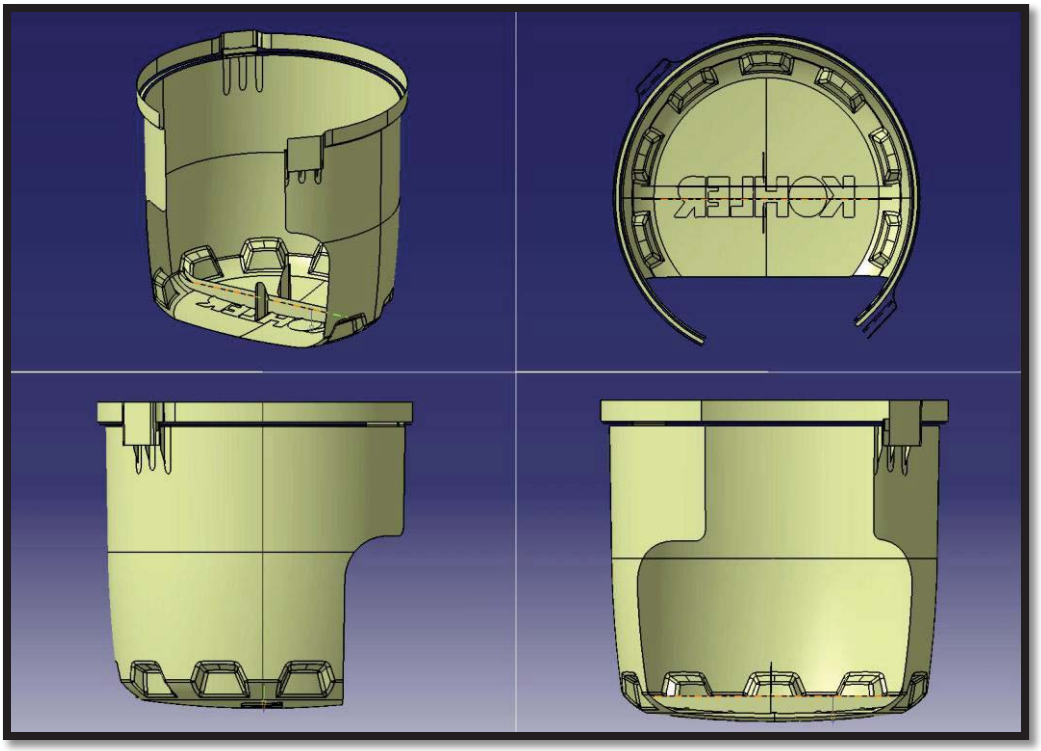

Figure 4.4: The Closed End Caps simplified 3D CAD model

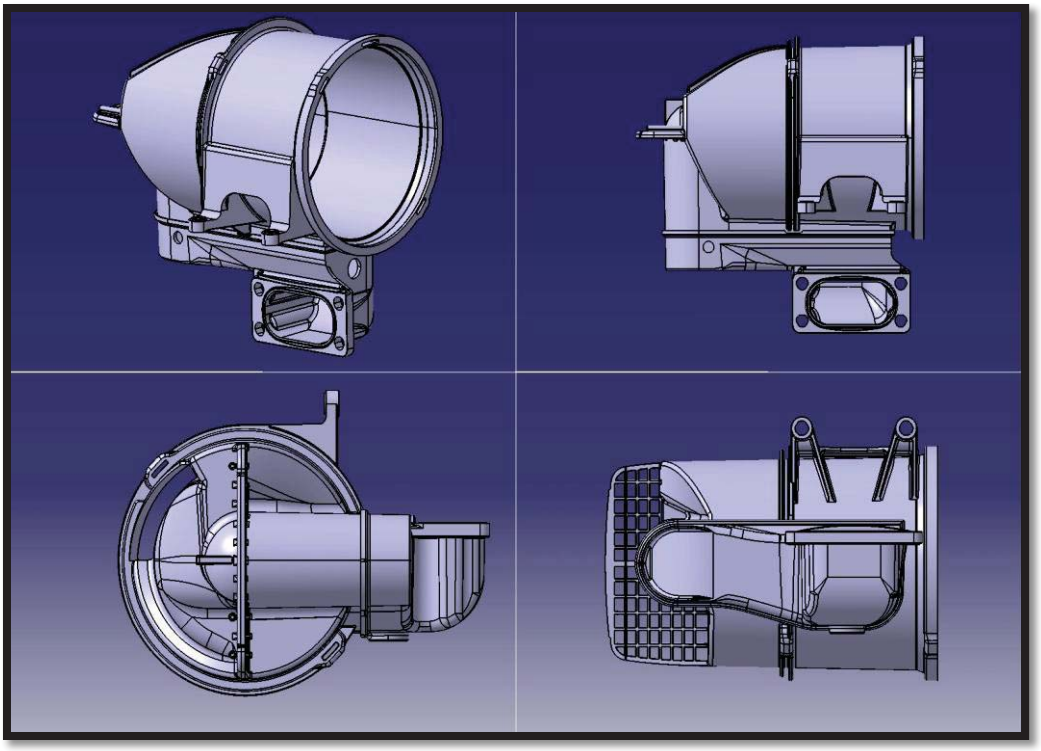

Figure 4.5: The Center Sections original 3D CAD model

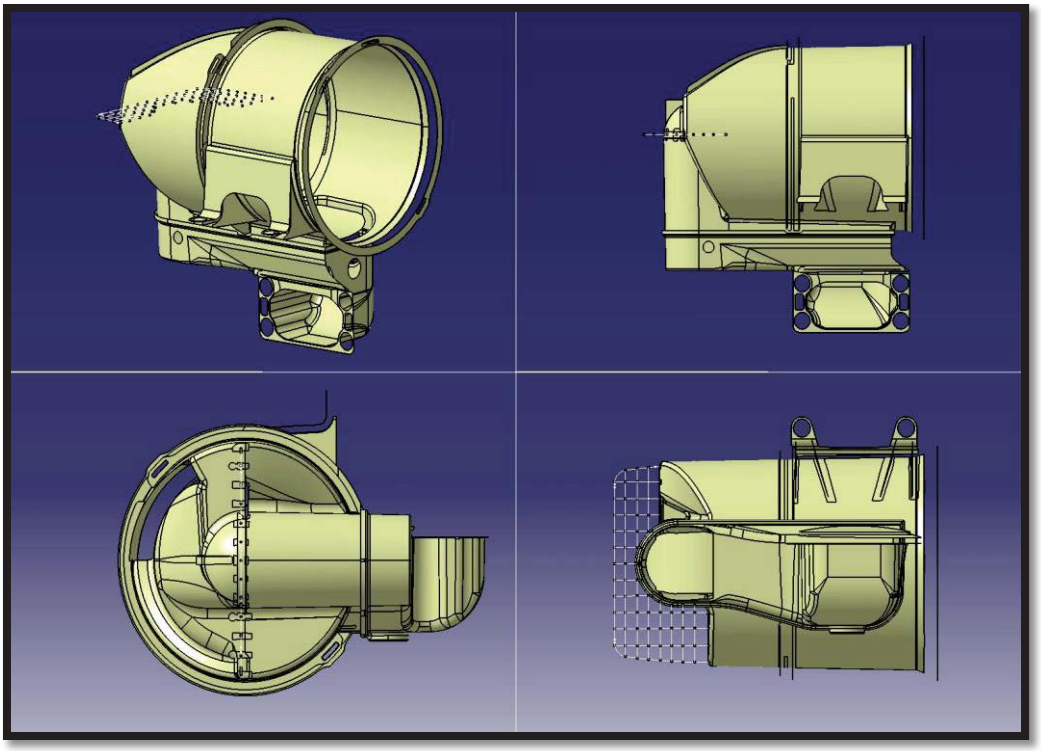

Figure 4.6: The Center Sections simplified 3D CAD model

4.1.2 Finite Element Model Mesh's

Using the simplified CAD models, FE model meshes were created using 1D and 2D elements. Figures 4.7 through 4.9 show the meshes for each part and table 4.1 shows the global element composition of each model. The 1D and 2D elements are realized using beam and shell properties, respectively. Element geometric quality checks were used during mesh creation to avoid a poorly conditioned model. A sample of these element quality checks for each model is shown in tables 4.2 through 4.4.

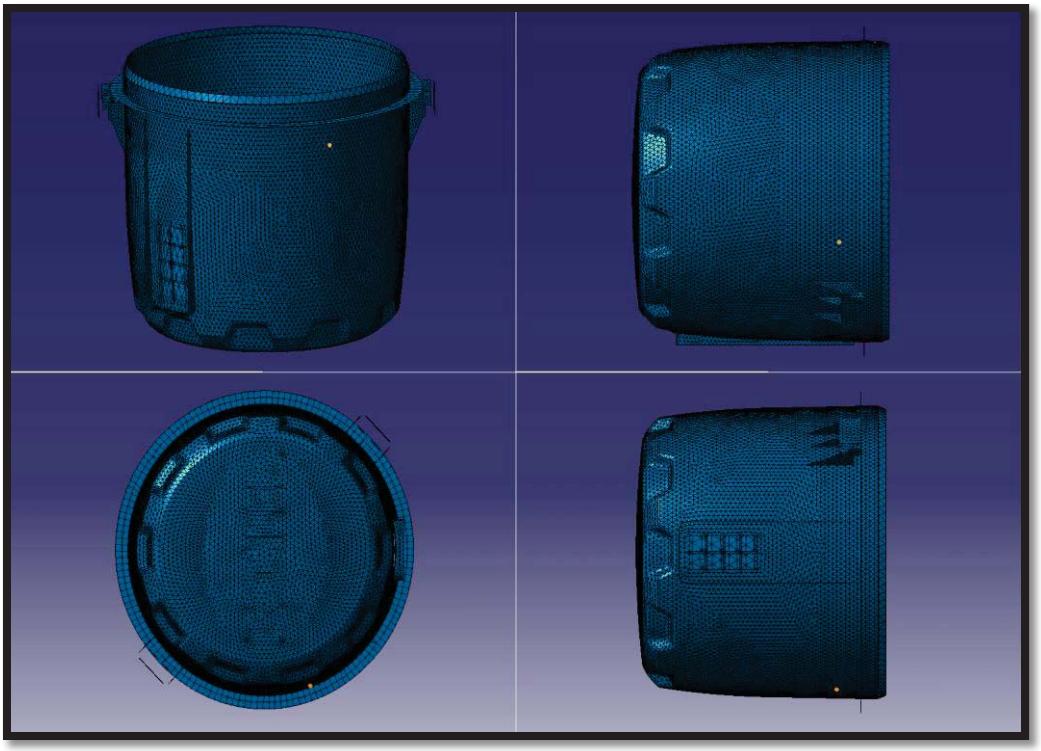

Figure 4.7: FE model mesh for the Open End Cap

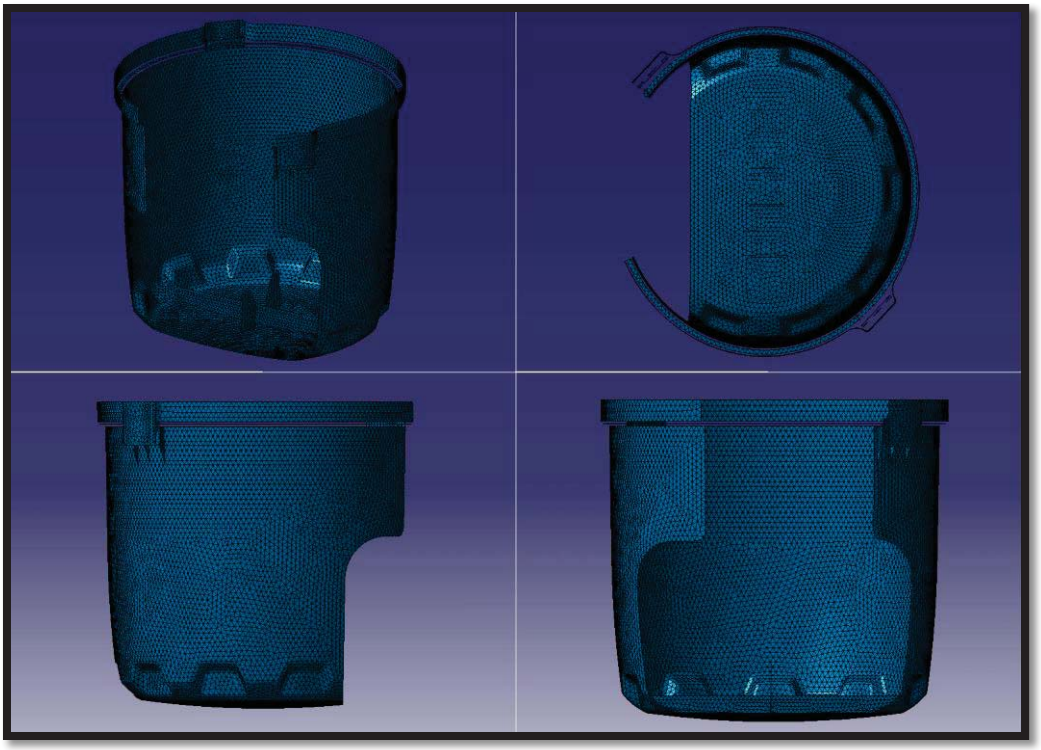

Figure 4.8: FE model mesh for the Closed End Cap

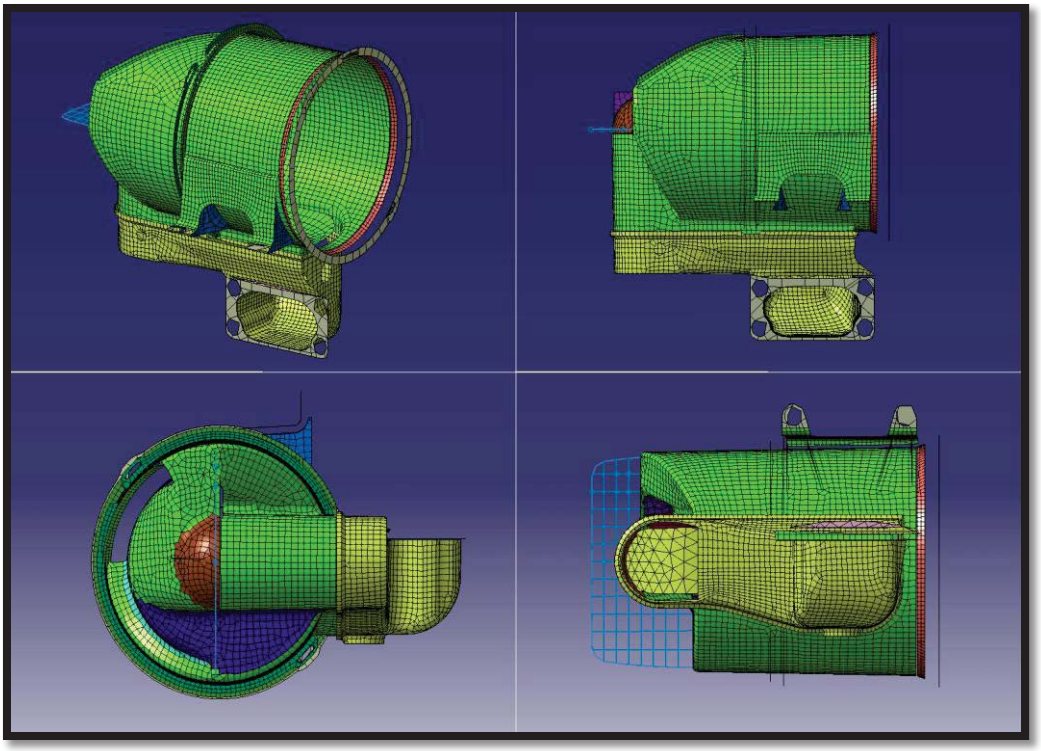

Figure 4.9: FE model mesh for the Center Section

Table 4.1: FE model global mesh composition and element types

Part No.	Global Mesh Composition		Element Types (# of Elements)						Nominal Element Size (mm)
	Total Number of Nodes	Total Number of Elements	Bar	Beam	TRIA3	TRIA6	QUAD8	Rigid Spider	
6209401	35461	13616	32	144	0	721	10357	2362	2.5-10
6209625	48707	25008	0	0	0	23532	0	1476	2.5-3.009
6209622	57041	31045	0	0	1158	27157	300	2430	2.5-5

Table 4.2: FE model mesh geometric quality statistics for the Open End Cap

Quality Criteria	Good	Poor	Bad	Worst	Average
Stretch	28311 (99.99%)	4 (0.01%)	0	0.277	0.942
Min. Angle Tria. (deg)	28245 (99.75%)	68 (0.24%)	2 (0.01%)	13.735	54.968
Max Angle Tria. (deg)	28305 (99.96%)	10 (0.04%)	0	142.307	65.469
Min. Angle Quad. (deg)	300 (100%)	0	0	67.682	86.973
Max. Angle Quad. (deg)	300 (100%)	0	0	113.18	93.030
Aspect Ratio	28601 (99.95%)	14 (0.05%)	0	3.157	1.119
Global	28544 (99.75%)	69 (0.24%)	2 (0.01%)	N/A	N/A

Table 4.3: FE model mesh geometric quality statistics for the Closed End Cap

Quality Criteria	Good	Poor	Bad	Worst	Average
Stretch	23521 (99.95%)	10 (0.04%)	1 (0.004%)	0.034	0.94
Min. Angle Tria. (deg)	23506 (99.89%)	17 (0.07%)	9 (0.04%)	1.163	54.868
Max Angle Tria. (deg)	23521 (99.95%)	11 (0.05%)	0	145.508	65.759
Aspect Ratio	23515 (99.93%)	9(0.04%)	8 (0.04%)	38.119	1.127
Global	23504 (99.88%)	19 (0.08%)	9 (0.04%)	N/A	N/A

Table 4.4: FE model mesh geometric quality statistics for the Center Section

Quality Criteria	Good	Poor	Bad	Worst	Average
Stretch	716 (99.31%)	5 (0.69%)	0	0.164	0.834
Min. Angle Tria. (deg)	694 (96.36%)	21 (2.91%)	6 (0.83%)	6.06	46.598
Max Angle Tria. (deg)	713 (98.89%)	8 (1.11%)	0	143.154	75.064
Min. Angle Quad. (deg)	10232 (98.79%)	109 (1.05%)	16 (0.15%)	39.842	83.016
Max. Angle Quad. (deg)	10206 (98.54%)	120 (1.16%)	31 (0.3%)	139.968	97.03
Aspect Ratio	10875 (98.17%)	166 (1.5%)	37 (0.33%)	62.696	1.321
Global	10705 (96.63%)	295 (2.66%)	78 (0.7%)	N/A	N/A

4.2 Experimental Modal Analysis Set-Up

As stated above the experimental modal analyses were performed using an approximation to the free-free boundary condition. This approximation is specific to each part, depending on the test stand that was used; these stands are described below. The frequency range and number of response measurement locations also vary, depending on the expected mode shapes. These expected mode shapes were determined through the analytical modal analyses, which were always, at least roughly, completed before the experimental modal analysis was performed.

A common element between each modal test was the excitation technique, which was a roving impact. This technique was chosen because it does not constrain the test objects motion (which a shaker can do) and its ease of use for modal tests with several measurement points. The impact hammer that was used in the described tests has a flexible handle so that it can be "flicked" into the structure unlike a traditional hammer, which must be swung. By holding onto this hammer with a clamp and "flicking" it into the structure, very repeatable and controllable impacts are possible. This was necessary for the modal tests

described below because of the materials non-linear behavior. An example of this hammer set-up can be seen in Figure 4.13 and Figure 4.15. The measurement transducers for each modal test also shared the same model numbers; these are shown below in table 4.5.

Table 4.5: The measurement transducers used in each modal test

Type	Model #	Description
Impact Hammer	PCB 086E80	Miniature impact hammer with flexible handle
Triaxial Accelerometer	PCB 356A13	Miniature (1gm) triaxial ICP type accelerometer
Single Axis Accelerometer	PCB 352A10/352M52	Miniature (0.7gm) ICP type accelerometer

4.2.1 Open End Cap Experimental Modal Analysis Set-Up

Figure 4.10 below shows the test stand used for the closed end caps modal test. The foam columns are used to hold up the structure by an internal ring, which is highlighted in red. These foam columns were used because they allow for a controllable modal test, due to the steadiness of the columns. This steadiness creates a much more consistent FRF when compared to other fixture methods (e.g. surgical tubing).

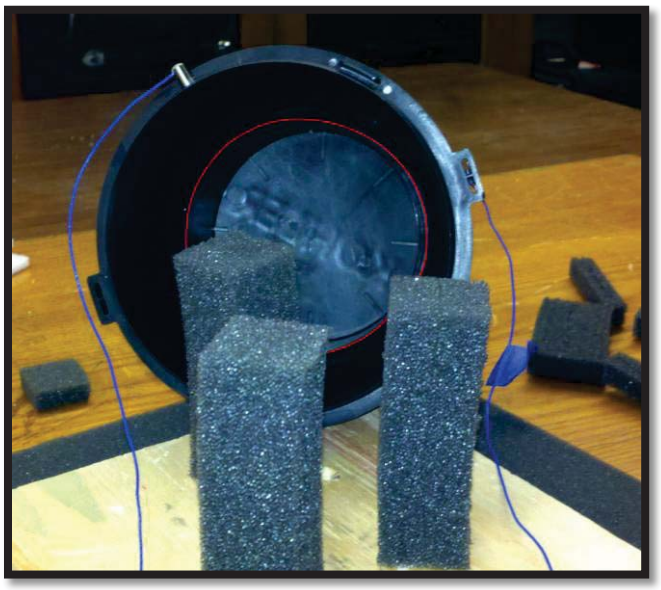

Figure 4.10: The Open End Caps modal test stand

These foam columns can introduce some experimental error because of the stiffness and damping they add to the system. This can correspondingly raise the natural frequencies and damping ratios of the system, most noticeably in the rigid body modes. The effects on the modes of interest are deemed to be negligible because of the foam columns locations. They support the inner ring, whose flexible motion was assumed to have a minimal impact on the modes of interest. It is also important to make sure that the rigid body modes are adequately separated from the systems modes. Figure 4.11 shows that there is approximately 15.5:1 separation. This is enough separation to avoid seeing the effects of the rigid body modes in the modes of interest.

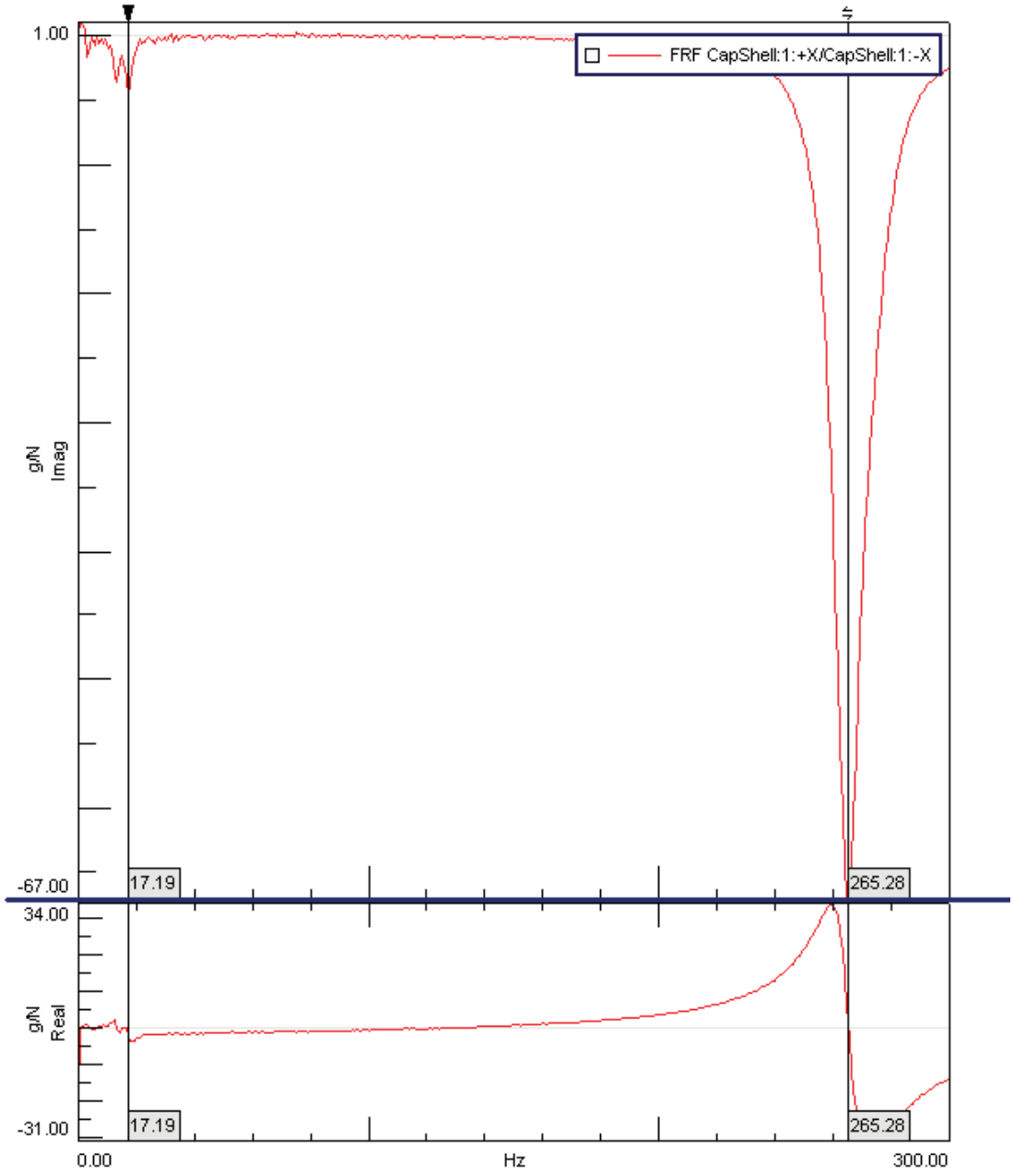

Figure 4.11: Open End Caps shell driving point FRF. The cursors show the location of the highest frequency rigid body mode and the lowest frequency system mode.

Figure 4.12 shows the test point arrangement. There are a total of 151 test points on the structure, 108 points on the shell and 43 on the top. Figure 4.13 is a picture of the complete modal test set-up. Three accelerometers were used in the modal test; two were placed asymmetrically on the rim of the shell and one off center on the top. Again, the

measurement points were chosen based on the mode shapes that were predicted in the analytical modal analysis.

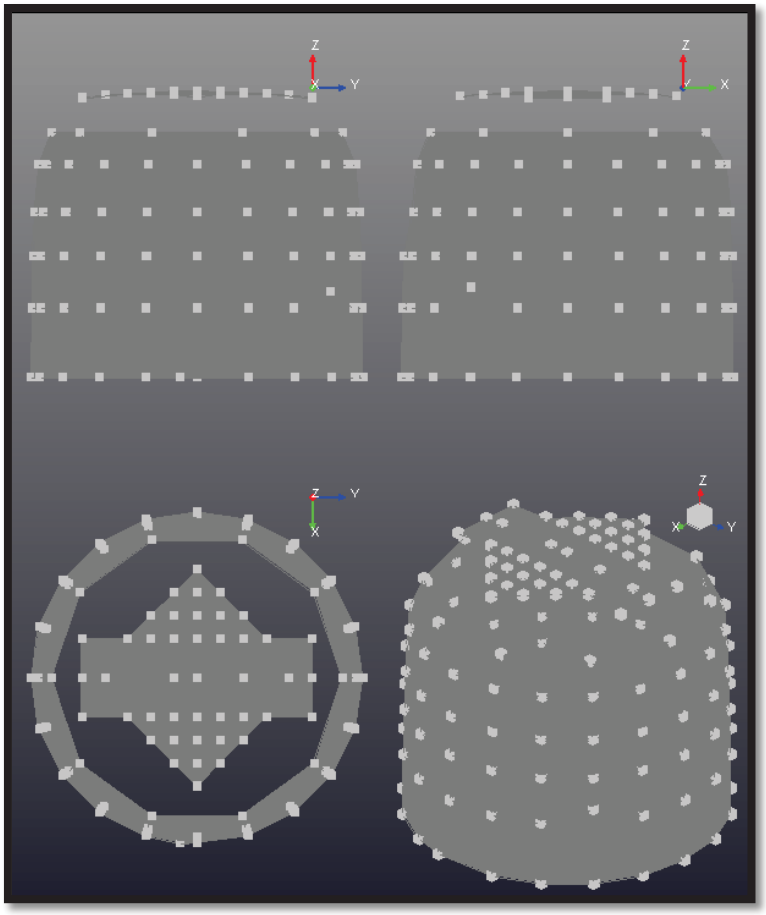

Figure 4.12: Modal test point arrangement for the Open End Cap

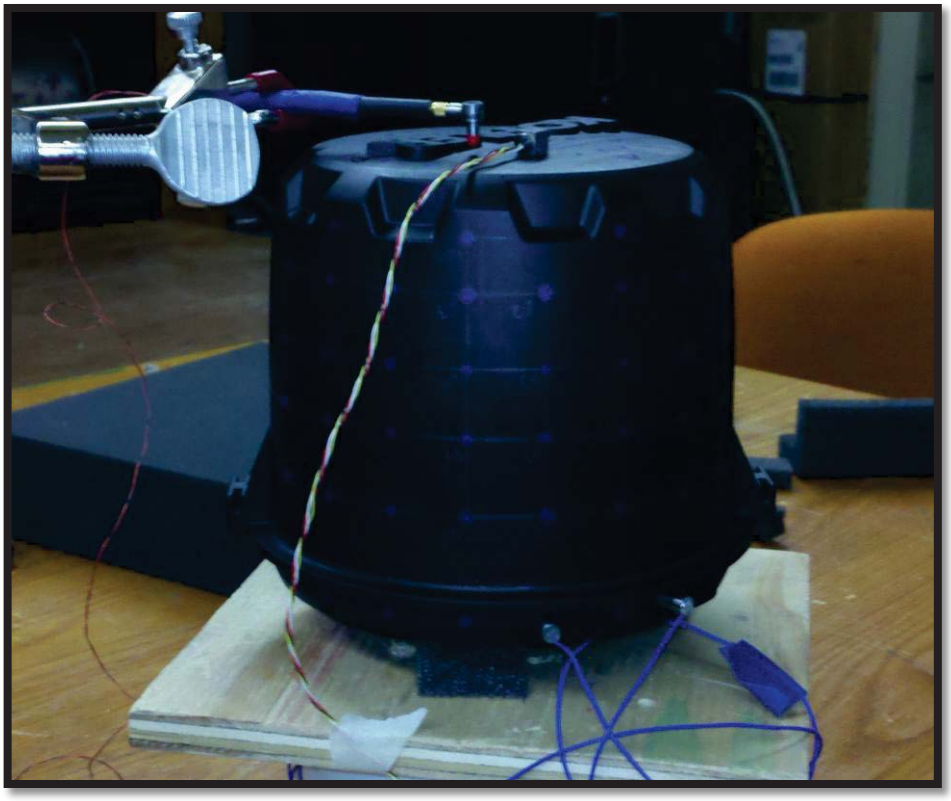

Figure 4.13: The Open End Caps complete modal test set-up

4.2.2 Closed End Cap Experimental Modal Analysis Set-Up

Figure 4.14 shows the test stand used for closed end caps modal test and Figure 4.15 shows how the test stand and part were set-up for the test. The foam test stand was used for the same reasons as for open end caps modal test.

Figure 4.14: Closed End Caps modal test stand

Part 4.15: Closed End Cap modal test stand set-up

Also as before, this test stand will introduce some experimental error to the measurements because of the foams stiffness and damping. The foams effects on the modes of interest are minimal; this is because it supports the part at node points for the modes of interest. The rigid body modes can still be heavily affected by the test stand; this makes it necessary to ensure they will not affect the systems flexible modes. Examining Figure 4.16 shows that there is approximately 9:1 separation between the lowest system mode and the highest rigid body mode. This is deemed to be enough to avoid the rigid body modes affecting the systems modes

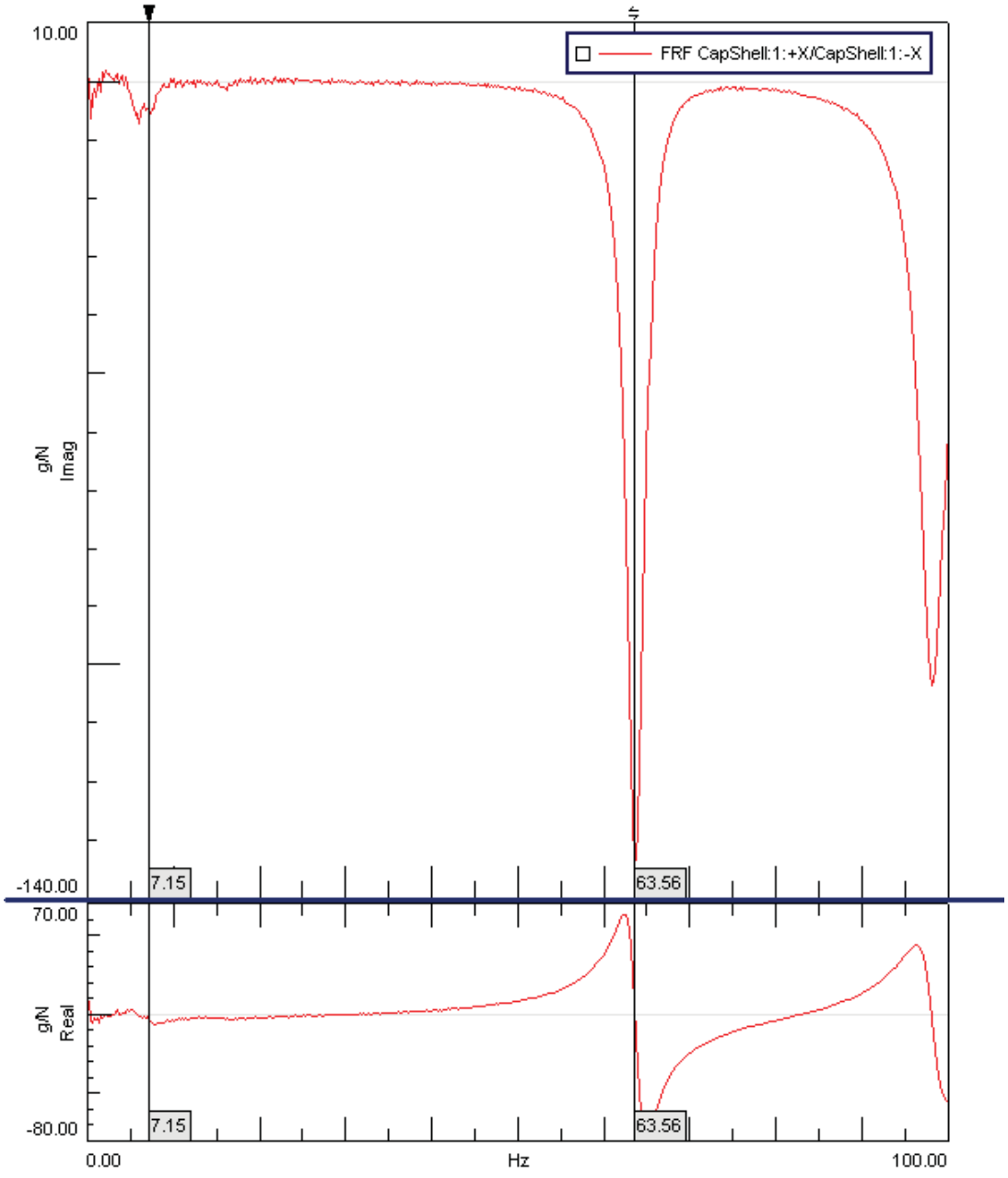

Figure 4.16: Closed End Cap shell driving point FRF. The cursors show the location of the highest frequency rigid body mode and the lowest frequency system mode.

Figure 4.17 shows the test point arrangement for closed end caps modal test. A total of 172 test points were used with 122 points on the shell and 50 points on the top. The test points on the shell are evenly distributed around its circumference with 7 different levels. The test points on the top were distributed into 7 rows with the majority of the points being

concentrated towards the open end of the shell. This was done because that is where most of the motion was expected based on the FE models modal solution.

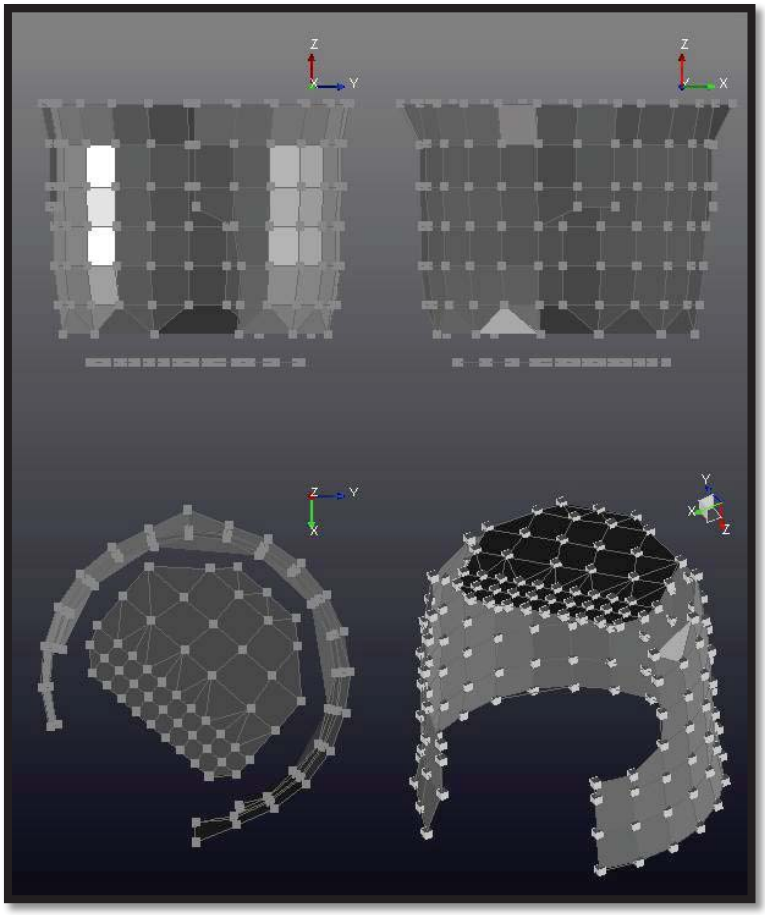

Figure 4.17: Modal test point arrangement for the Closed End Cap

The complete modal test set-up is shown in Figure 4.18. Only two accelerometers were used in this modal test. One was placed on the edge of the shell and the other was placed off center on the open edge of the top. As before, the accelerometers were placed in these locations based on the analytical modal analysis.

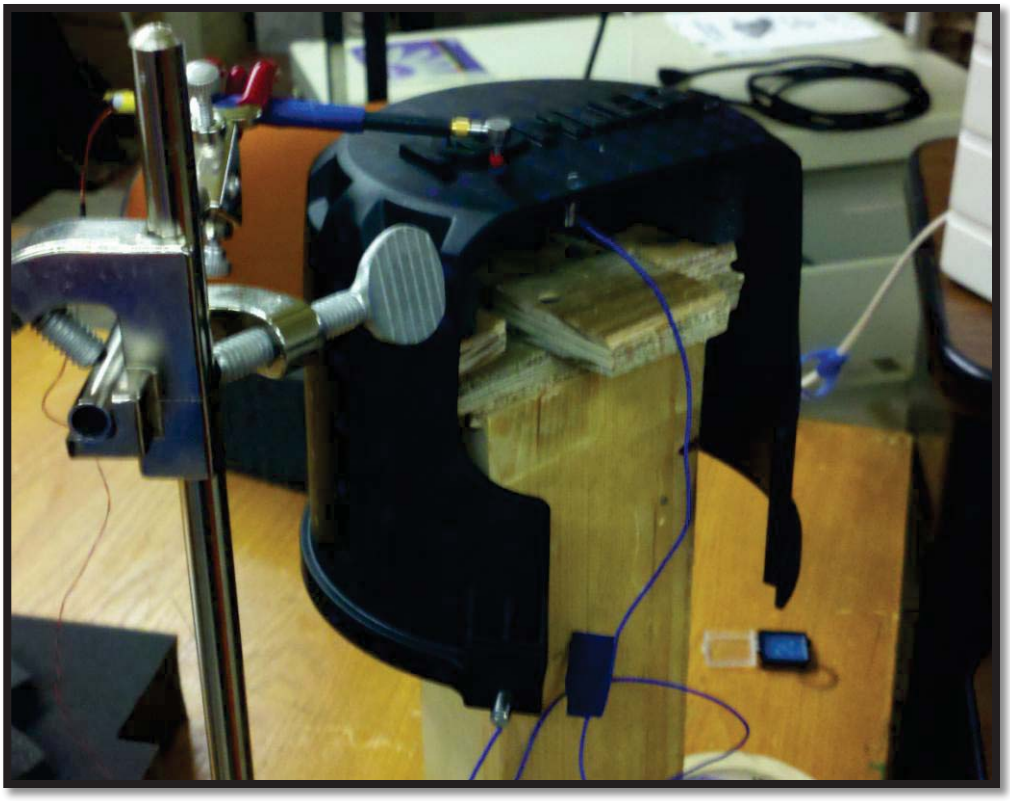

Figure 4.18: The Closed End Caps complete modal test set-up

4.2.3 Center Section Experimental Modal Analysis Set-Up

A picture of the modal test set-up can be seen in Figure 4.19 and the test point arrangement can be seen in Figure 4.20. There are a total of 387 test points distributed somewhat evenly on the part. Four accelerometers were used for the test. As in the other modal analyses a subjective pre-test analysis was done using the FE model in order to qualitatively determine the measurement transducer locations. These were chosen based on the high amount of predicted motion. In this test, surgical tubing was used in order to approximate the free-free boundary condition. Unlike in the previous modal tests, this part has sufficient mass to the point that it will not move excessively after impacts, meaning that the modal test will still be controllable and consistent.

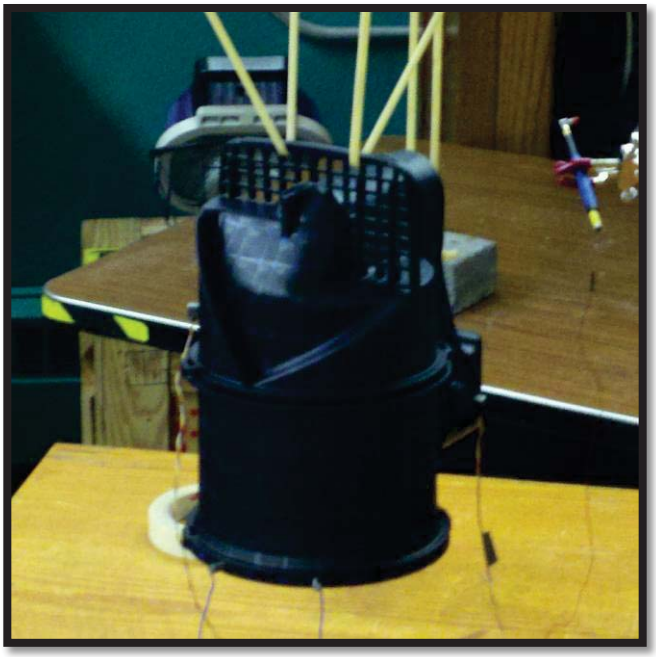

Figure 4.19: The Center Section's complete modal test set-up

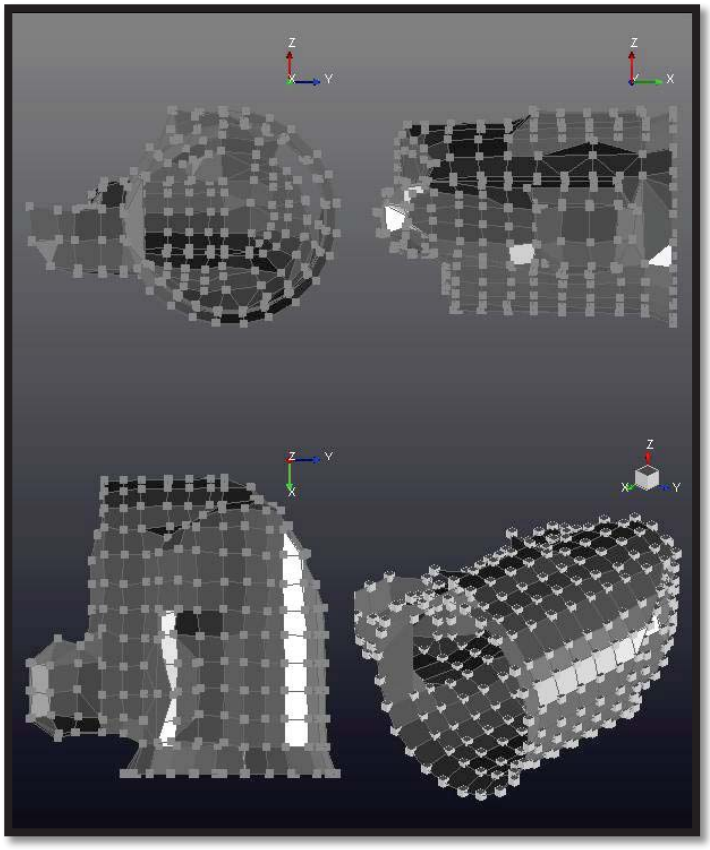

Figure 4.20: Modal test point arrangement for the Center Section

Chapter 5: HDAC Assembly Analysis Set-Up

The assembled HDAC was analyzed two different ways. An analytical and experimental modal analysis was performed as well as a dynamic response prediction/measurement. These analyses were done to perform a test-analysis model correlation and calibration as well as to assess the assembled FE models predictive capabilities. This chapter will discuss how the assembled FE model and HDAC were set-up for these analyses. The test fixtures, transducer set-up, and excitation techniques will be explained for the experimental case. While the connection properties and simulation set-up will be discussed for the analytical case. For the data acquisition set-up parameters refer to appendix A in chapter 9.

The test-analysis model correlation and calibration was done twice for the assembled system, with and without the air filters in the HDAC. This was done in order to isolate the significant amount of uncertainty that the air filters introduce to the FE model. Isolating this uncertainty should make the model correlation and calibration process simpler and easier

5.1 Assembled HDAC Experimental Analysis

Two different experimental methods were used to perform the analyses mentioned above. For the modal analysis a roving impact hammer test was used. The dynamic response measurement was done using a shaker test with a broadband random input.

5.1.1 Assembled HDAC Modal Analysis

The modal analysis performed on the assembled HDAC followed the same procedure as was used for each of the individual components. Also as before, the system was tested using a free-free boundary condition; this was approximated by hanging the HDAC with surgical tubing. Figure 5.1 below shows the test point configuration used for

this analysis. A total of 77 test points were used, 22 points were on the closed end cap, 23 points on the open end cap, and 32 points on the center section. These modal test points were in the same locations on the individual components as the previous modal tests. Fewer test points were used however, because this analysis was only to get a rough idea of what the assembled HDAC's modal properties are. This means that a fine test point resolution was not necessary. As with all the previous tests, these points were chosen based on where large amounts of motion were expected based on the FE models predictions.

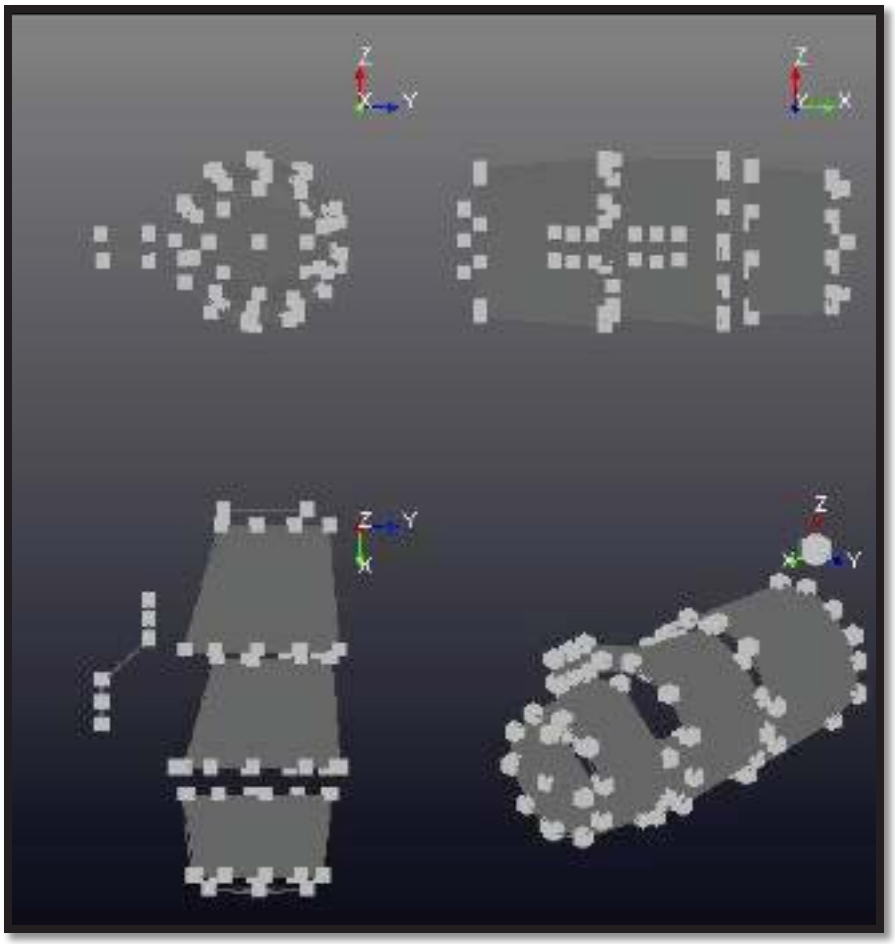

Figure 5.1: Modal test point arrangement for the assembled HDAC

The test set-up can be seen below in Figure 5.2. The same transducers as listed in table 4.5 were used in this test; four triaxial and two uniaxial accelerometers were used. It

should be noted that two of the triaxial accelerometers placed on shells of both the end caps only measured the acceleration normal to the surface (only one channel was used). The reason for using the triaxial accelerometers was because a miniature accelerometer was desired but the supply of miniature uniaxial accelerometers was limited. As with the test points the measurement locations were chosen based upon where large amounts of motion were expected.

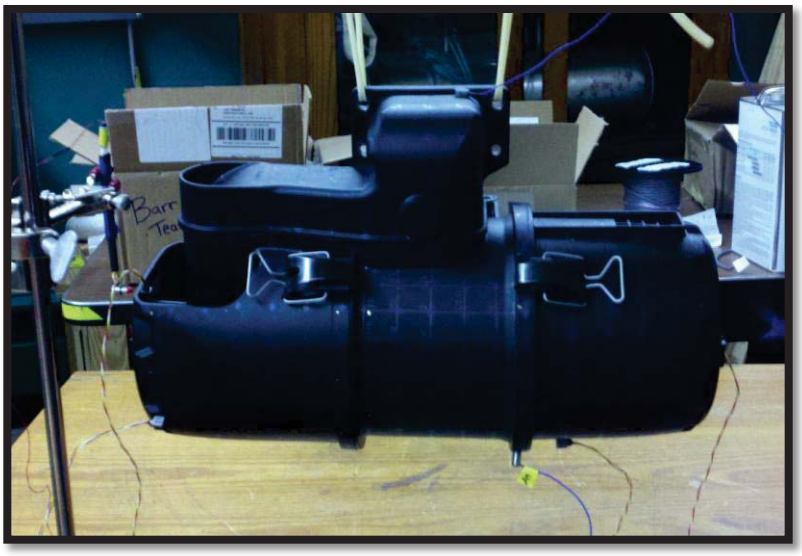

Figure 5.2: Assembled HDAC complete modal test set-up

It should also be noted that the unsupported corner of the closed end cap was glued to the center section. This was done in order to stop it from rattling during the modal test. It is understood that this modifies the original structure and will change the systems modal parameters, but it is a consolation that must be made in order to perform the analysis.

5.1.2 Response Measurement Shaker Test Set-Up

The systems experimental response was found through shaker testing, which simulates actual use. To do this, the HDAC was mounted using a fixture that imitates its normal boundary conditions; this fixture is shown below in Figures 5.4 and 5.5. The system

was excited through the base of the fixture, using broadband random vibration. The input spectrums can be seen below in Figures 5.9 And 5.10.

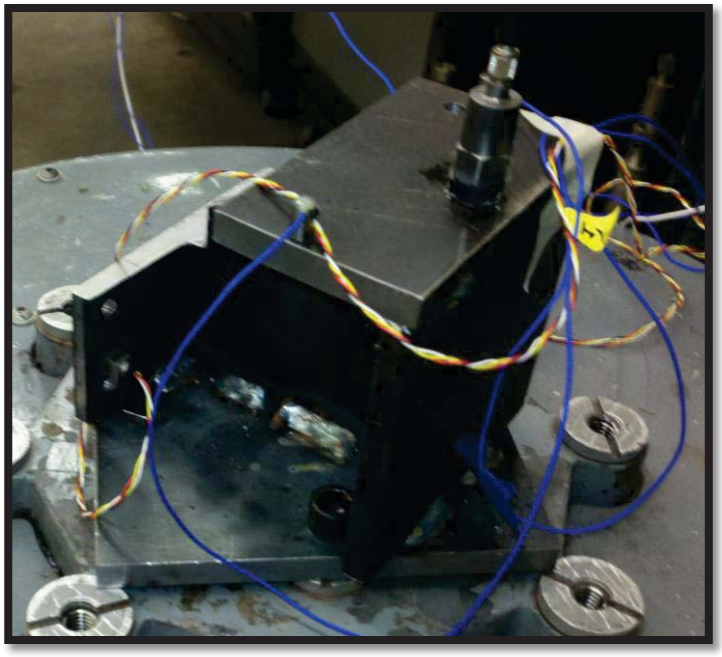

Figure 5.4: Picture of the model validation experiment test fixture from the back right side

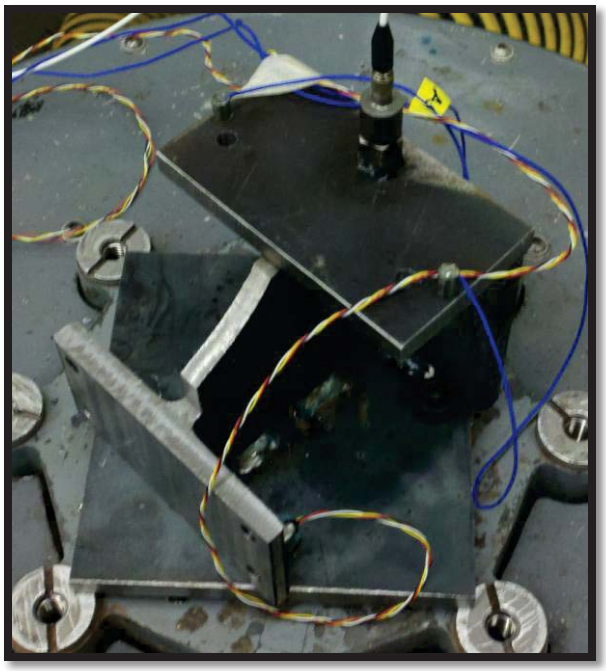

Figure 5.5: Picture of the model validation experiment test fixture from the front right side

In order to avoid any artificial amplification or attenuation due to resonances in the fixture, its rigidity was checked before any testing took place. This was done using random base excitation with a flat PSD and ensuring that the resulting frequency response is constant over the desired range. Two different reference locations were used during this check; one reference was on the shakers armature and the other was the control transducer (the large accelerometer on the top of the fixture). Three different response transducers were used in this check and were at three HDAC mounting points; both the left and right bolt holes on the top of the fixture and in between the top and bottom bolt holes on the front right of the fixture. The resulting FRFs are shown below in Figures 5.6 and 5.7.

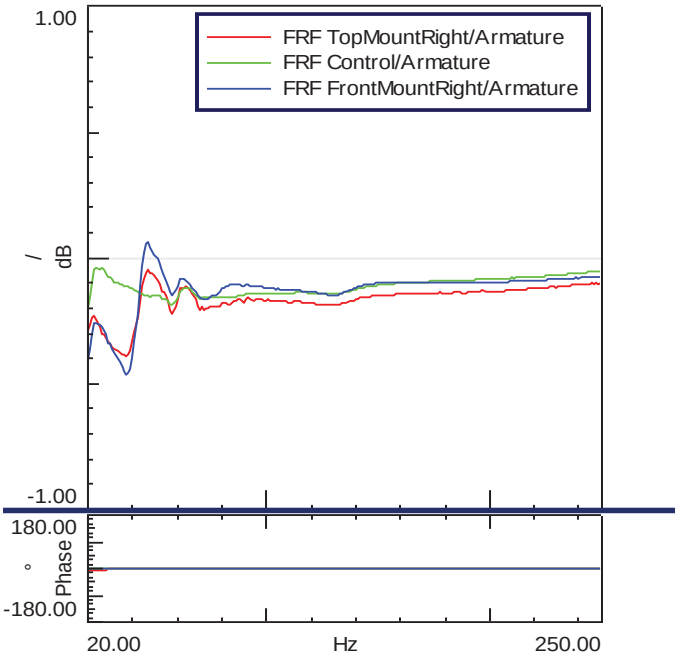

Figure 5.6: FRF's for various points of the test fixture when referenced to the shakers armature (dB reference = 1)

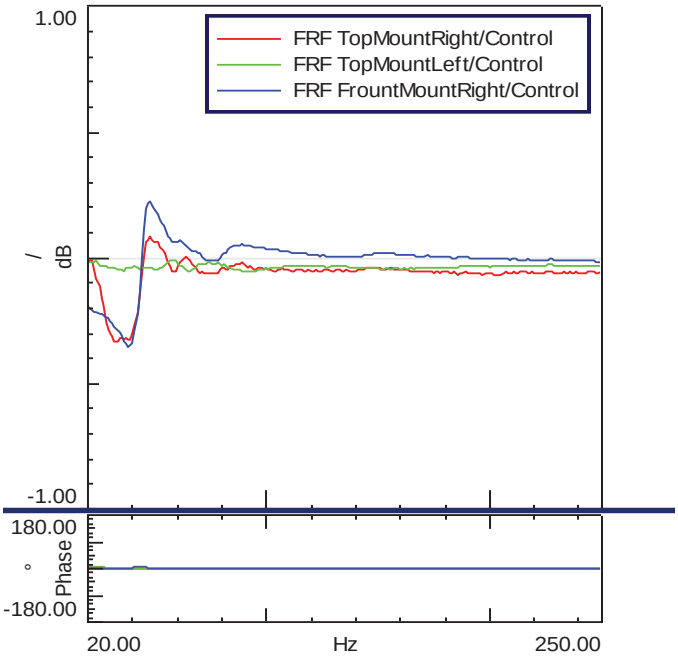

Figure 5.7: FRF's for various points of the test fixture referenced to the control accelerometer (dB reference = 1)

The above plots show that the fixture is sufficiently rigid for this test. There are virtually zero phase differences between the different mounting points and the armature or control point. However, there are some slight magnitude differences, which are deemed to be a simple impedance mismatch. These magnitude differences are deemed to be acceptable because of how small they are, with only about +/- 0.25 dB of variance around a mean value of zero. It is also somewhat important to recognize that because the FRF's magnitudes are slightly below zero dB, some of the excitation is being dissipated in the fixture.

Figure 5.8 below shows the HDAC's test set-up for the response measurement. Three accelerometers were used in this test, one per each main plastic component. The accelerometers are the same models listed in table 4.5. Two uniaxial accelerometers and one triaxial accelerometer was used, similar to the modal analysis the triaxial accelerometer was used for its small size and only measured the acceleration normal to the parts surface. Again,

the measurement points were chosen based on where large amounts of motion were expected.

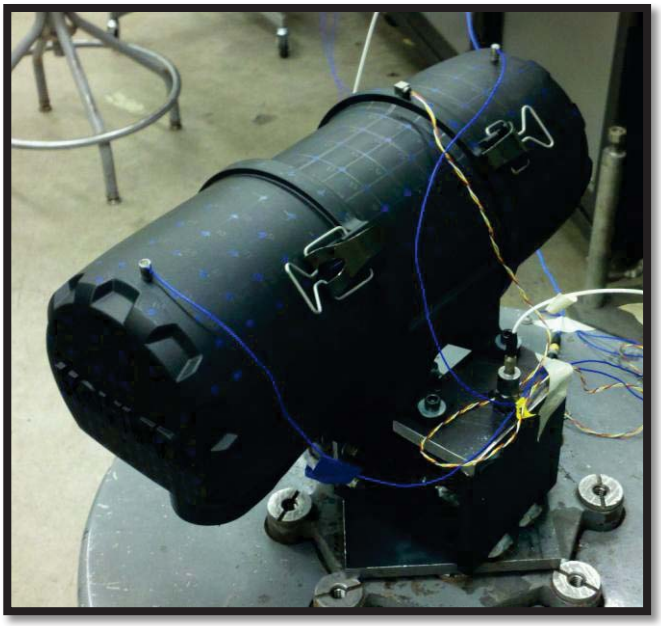

Figure 5.8: Validation experiment test set-up

5.1.3 Shaker Test Input Frequency Spectrums

Two different excitation frequency spectrums were used for the model validation; one spectrum was held at the same level for the entire frequency range (shown in Figure 5.9), and another, which is more representative of the operating conditions (shown in Figure 5.10), which takes its inspiration from an outdated durability test standard from Kohler Co. These two different spectrums where used to provide a "simple" and "complex" input spectrum, respectively. The "simple" spectrum was used in order to help understand the simulation and further calibrate the assembled model (primarily for connection damping). The "complex" spectrum was used to perform the models blind prediction to assess its predictive capabilities. Additionally the HDAC's response was measured at different load levels by scaling the input spectrums overall RMS level.

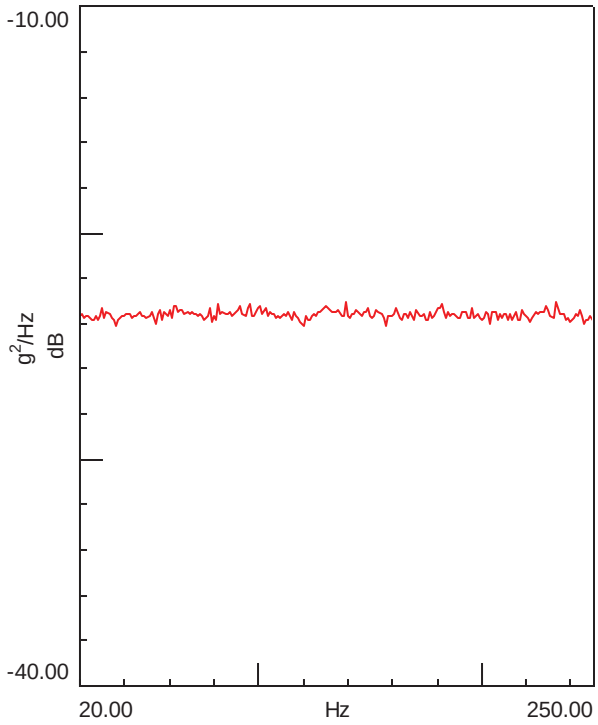

Figure 5.9: Model validation experiment flat test profile PSD (dB reference = 1 g^2/Hz)

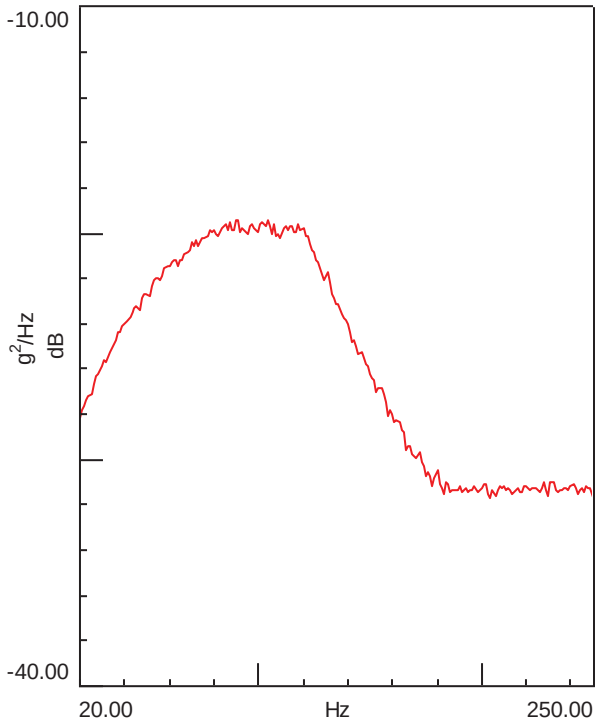

Figure 5.10: Model validation experiment "complex" test profile (dB reference = 1 g^2/Hz)

5.2 HDAC FE Model Assembly Analysis

The assembled HDAC's FE model analysis attempts to imitate the physical experiments as best it can. This includes the boundary conditions and input spectrums. The FE model boundary conditions are idealized versions of the test boundary conditions. For the response prediction the exact inputs used in the shaker test were used as the input spectrum. This was done by measuring the experimental input with the control accelerometer, the spectrums used are shown above in Figures 5.9 And 5.10.

5.2.1 HDAC FE Model Assembly

The HDAC's component FE models were assembled using the connection locations shown below in Figure 5.11 (displayed by the white markings). These locations were chosen based on two criteria, simplicity of application and how realistic they are. It is important to note that the connections represent contact rather then the actual assembly of the HDAC. This was done in order to simplify the FE model instead of modeling the actual connections, which would require much more sophisticated techniques. Based on engineering judgment it was hypothesized that this would be acceptable to meet the objectives of the project.

To model the interfaces, bush connections were used because of their simplicity and how easy it is to modify their damping and stiffness properties. By adjusting these properties the connections can be approximated more accurately. Other connection types are available, but either do not allow for the same type of customization as the bush connector or are unnecessarily complex for this models purpose. The connection properties (stiffness and damping), which will be used for the blind response prediction, will be found during the model calibration and are described in chapter 9 appendix C.

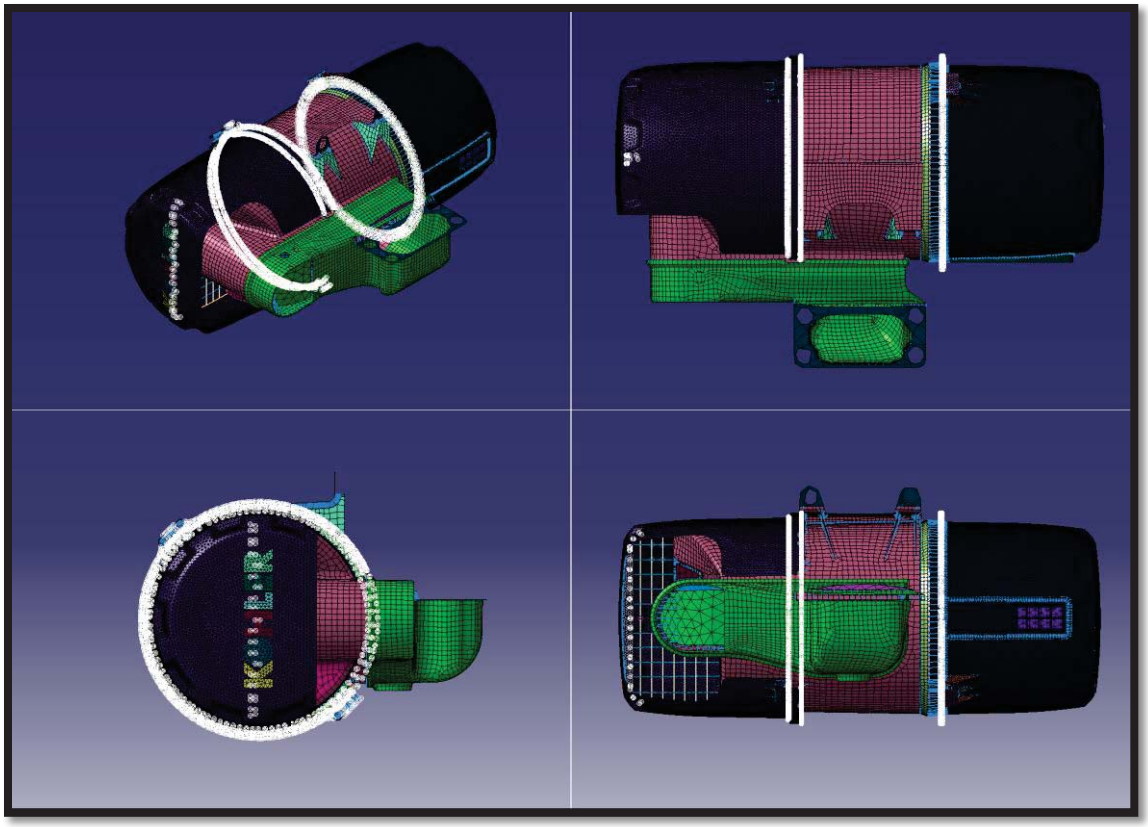

Figure 5.11: The assembled HDAC FE model connection locations, the connections are shown by the white markers

The filters effects on the system were modeled using a simple FE model with one-dimensional beam elements. This was done in order to approximate the filters mass distribution in the HDAC. In order to approximate the filters material properties a "quick and dirty" model correlation and calibration was performed. The FE models density and Youngs modulus were adjusted until the its mass matched the measured mass, and its first natural frequency matched the first measured natural frequency. It should be noted that the filters stiffness was assumed to have a negligible effect on the HDAC; the stiffness was only adjusted to be in the ballpark of the physical systems. For more information on the filters FE model set-up refer to chapter 9 appendix D.

5.2.2 Assembled HDAC Analysis Types

The FE model described above was analyzed using MSC.Nastran. The modal solution was found using the same methods as was used for the individual components (normal modes SOL 103 – Lanczos) and ignores damping. The systems response was predicted using a frequency response analysis case with a frequency dependent enforced acceleration input. The response was calculated using modal parameters (SOL 111) instead of a direct calculation (SOL 108). For the frequency response case, damping was estimated using a structural damping coefficient, determined through the modal analysis and model calibration.

Chapter 6: Results and Analysis

This chapter presents the results from the analytical and experimental analyses described in the previous chapters. To do this, it is broken up into four sections to describe the results for the HDAC component and assembly modal analyses, the resulting test-analysis model correlations and calibrations, and the comparisons of the measured and predicted response spectrums used to assess the FE models predictive capabilities.

6.1 HDAC Component Modal Analyses and Model Correlation

This section will present the results from the analytical and experiment modal analyses as well as the model correlation of the HDAC components. The mode shapes, natural frequencies, damping ratios, and MAC values between corresponding modes will be shown. Since the FE models modal solution does not take damping into account, damping ratios will only be given for the experimental modes. Tables 6.1 through 6.7, 6.9 through 6.18, and 6.20 through 6.21 below show the corresponding analytical and experimental mode shapes and natural frequencies side by side. A short description of the mode shape is also provided in each tables label. Tables 6.8, 6.19, and 6.22 below are the mode pair tables for each component and show various comparisons between the modal properties of the corresponding modes.

The experimental mode shapes, which are shown below, were calculated assuming they were real-normal modes. This was done to ensure the experimental and analytical modal models share the same theoretical basis. The experimental mode shapes were also calculated using a complex model and it was found that, for the individual components, the real and complex modes were extremely similar.

6.1.1 The Open End Caps Modal Analysis

The results from the open end caps modal analyses are shown below in tables 6.1 through 6.7. The modes corresponding to the inner ring, which were found analytically, have been omitted because they were not measured during the experimental modal analysis. Table 6.8 is the mode pair table for the open end cap. Before the modal parameters were compared, the FE models mass (207g) was compared to the physical systems (201g). This error is considered negligible and is considered an initial indication of the FE models accuracy.

Table 6.1: The first mode shape of the open end cap. This mode shape shows the parts cross-section taking an oval shape.

	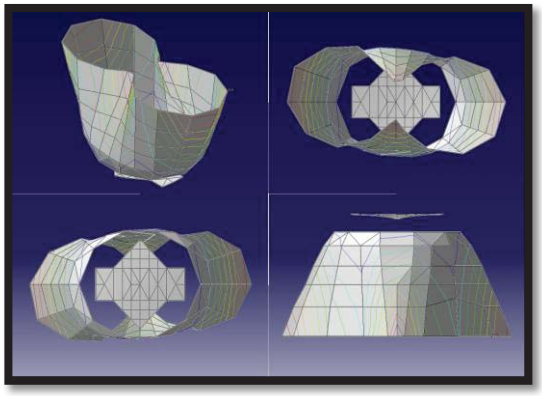
Analytical Modal Analysis ω_n=221.6 Hz	Experiment Modal Analysis ω_n=265.2 Hz ζ= 2.16%

Table 6.2: The second mode shape of the open end. This is a repeated mode shape of mode one, where the shape is slightly rotated.

	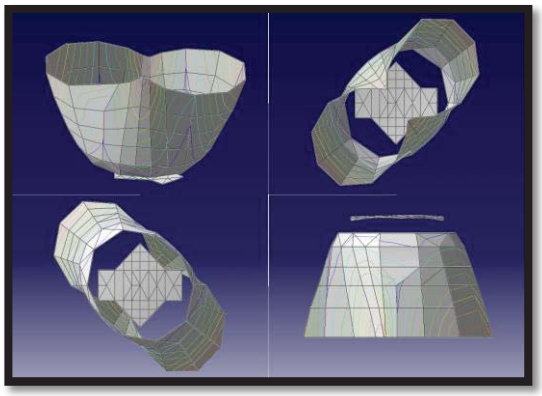
Analytical Modal Analysis ω_n=223.6 Hz	Experiment Modal Analysis ω_n=274.3 Hz ζ= 2.1%

Table 6.3: The third mode shape of the open end cap. This mode shape shows the parts cross-section taking a triangular shape.

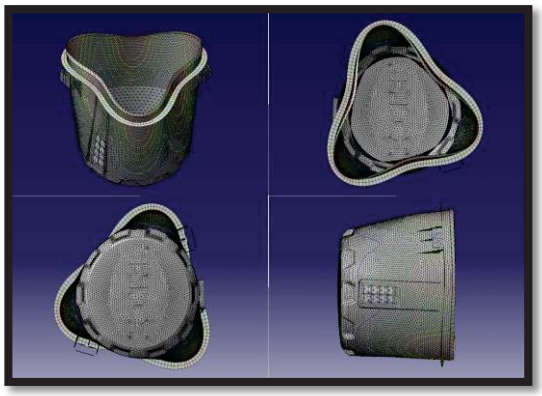	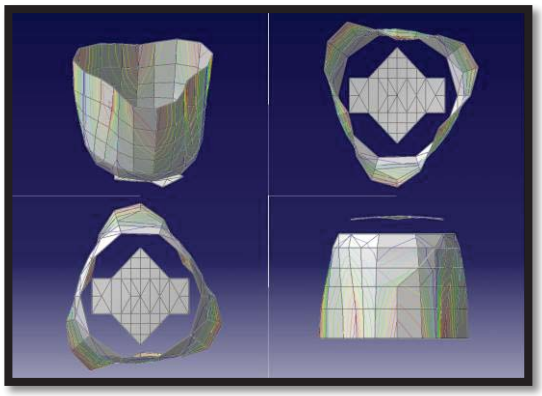
Analytical Modal Analysis ω_n=604.2 Hz	Experiment Modal Analysis ω_n=714.9 Hz ζ= 2.59%

Table 6.4: The fourth mode shape of the open end cap. This is a repeated mode shape of mode three, where the mode shape is slightly rotated.

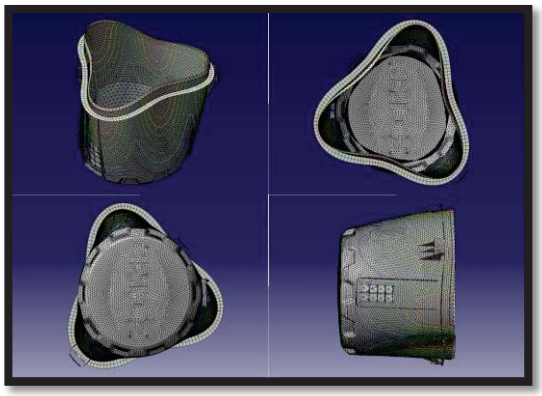	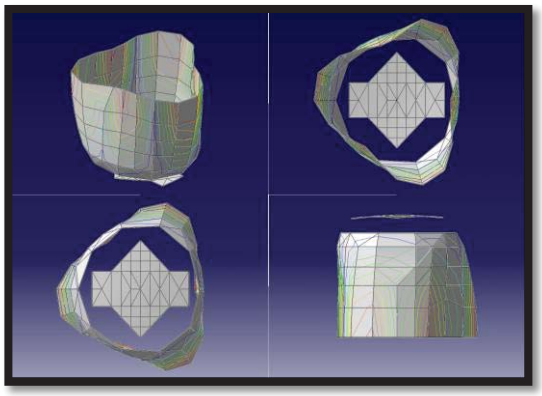
Analytical Modal Analysis ω_n=608.6 Hz	Experiment Modal Analysis ω_n=724.8 Hz ζ= 2.88%

Table 6.5: The fifth mode shape of the open end cap. This mode shape shows the bottom of the part flexing in and out.

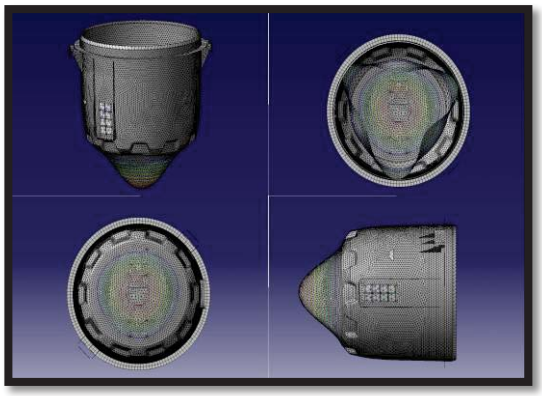	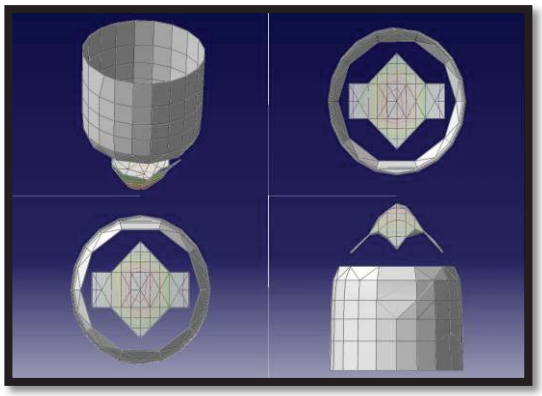
Analytical Modal Analysis ω_n=848.7 Hz	Experiment Modal Analysis ω_n=844.2 Hz ζ= 2.79%

Table 6.6: The sixth mode shape of open end cap. This mode shape shows the parts cross-section taking a square shape.

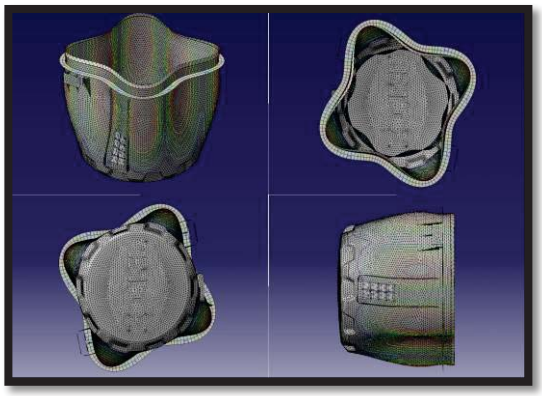	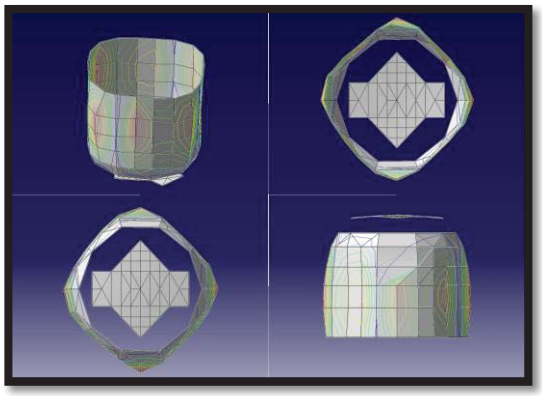
Analytical Modal Analysis ω_n=1052.2 Hz	Experiment Modal Analysis ω_n=1149.1 Hz ζ= 2.75%

Table 6.7: The seventh mode shape of open end cap. This is a repeated mode shape of mode six, where the mode shape is slightly rotated.

	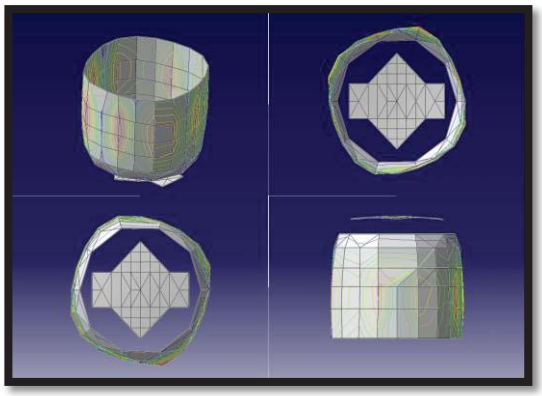
Analytical Modal Analysis ω_n=1058.7 Hz	Experiment Modal Analysis ω_n=1157.7 Hz ζ= 2.79%

Table 6.8: The Open End Caps original mode pair table

Test Mode ID	Frequency (Hz)	Finite Element Mode ID	Frequency (Hz)	MAC Value	Frequency Difference (Hz)	Frequency Difference (%)
1	265.2	7	221.6	0.853	43.69	16.5
2	274.3	8	223.6	0.846	50.7	18.5
3	714.9	9	604.2	0.654	110.68	15.5
4	724.8	10	608.6	0.643	116.24	16
5	844.2	13	848.7	0.989	4.56	0.5
6	1149.1	19	1058.7	0.923	90.36	7.9
7	1157.7	18	1052.2	0.913	105.5	9.1

Reviewing the tables above shows that the analytical and experimental modal analyses depict the same modes. This is evidenced by the similarity of the mode shape images and the high MAC values. Although it is difficult to see in the images above, close inspection of the mode shape images reveals that the shapes of modes one the four (the first two distinctive shapes), are rotated slightly different for analytical and experimental cases. This is not true for modes six and seven. This leads to the conclusion that the reason for the lower MAC values in modes one through four is likely because of the slight rotation differences.

The reasons for this difference in rotation lie in how symmetric the part is and the fact that anything, which effects that symmetry will change the mode shapes rotation. Because of this any defects or uncertainties in the parts construction will change its mode shape. The effects of the accelerometers mass were accounted for in the model, but this had a minimal effect because of their small size. It is hypothesized that this error is likely caused by uncertainty in the parts geometry (thickness distribution) or test fixturing. In the FE model, a true free-free boundary condition was used while the part was suspended using foam blocks in test. The external forces from this boundary condition most likely caused the differences in the mode shapes.

There are discrepancies in the comparisons between the analytically and experimentally found natural frequencies. Through these comparisons it is found that the analytical model under-predicts the natural frequencies. The reasons for these discrepancies is not exactly understood, possible reasons for error could be due to inaccurate material or geometric properties. This error will be minimized during the model calibration, where several experiments will be performed to reduce the frequency differences. The results are shown below in section 6.2.

6.1.2 The Closed End Caps Modal Analysis

Tables 6.9 through 6.18 below show the results from the closed end caps analytical and experimental modal analysis. Table 6.19 is the closed end caps mode pair table. An initial assessment of the FE models validity is confirmed by comparing its mass (157g) to the physical systems measured mass (156g). This small error is most likely due to the de-featuring of the model.

Table 6.9: The First mode of the closed end cap. This mode shape shows the open side of the part squeezing in and out.

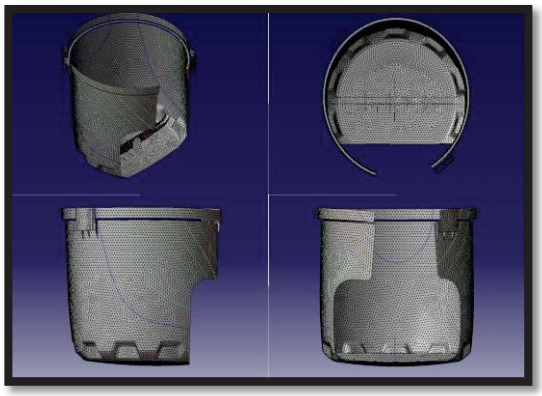	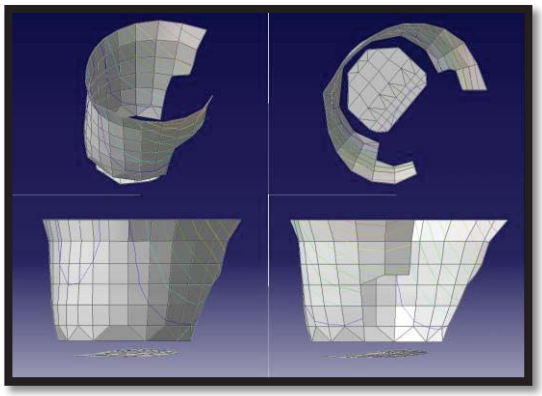
Analytical Modal Analysis ω_n=63.1 Hz	Experiment Modal Analysis ω_n=63.7 Hz ζ= 1.83%

Table 6.10: The second mode of the closed end cap. This mode shape shows the open sides of the part flexing side to side.

	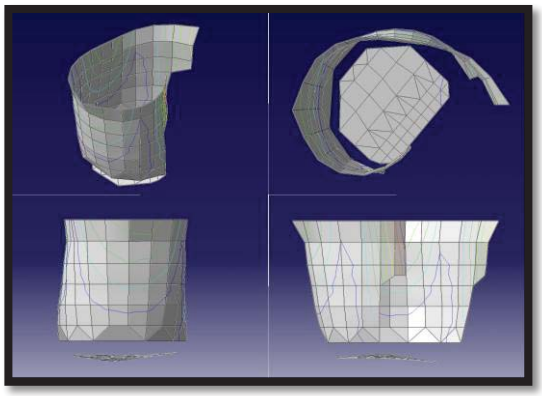
Analytical Modal Analysis ω_n=91.8 Hz	Experiment Modal Analysis ω_n=98.1 Hz ζ= 1.98%

Table 6.11: The third mode of the closed end cap. This mode shape shows the open sides of the part flexing side to side with a slight twist.

	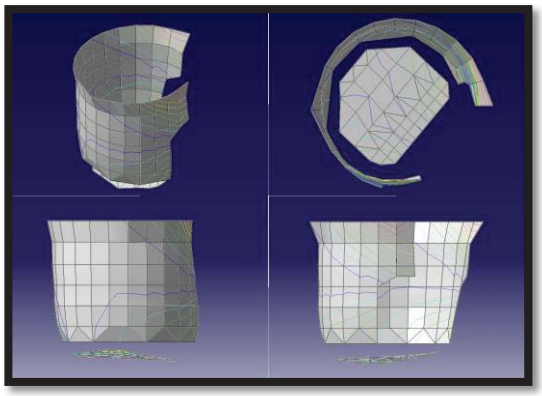
Analytical Modal Analysis ω_n=104.7 Hz	Experiment Modal Analysis ω_n=112 Hz ζ= 2.04%

Table 6.12: The forth mode of the closed end cap. This mode shows the parts cross-section taking a partial oval shape.

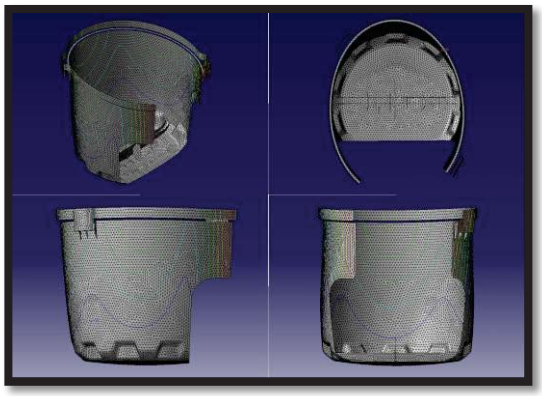	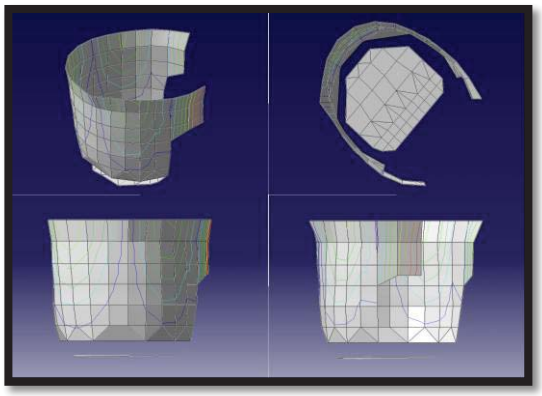
Analytical Modal Analysis ω_n=194.1 Hz	Experiment Modal Analysis ω_n=202.5 Hz ζ= 2.10%

Table 6.13: The fifth mode of the closed end cap. This mode shape shows the middle of the part bulging in and out, the top of the part is also flexing up and down.

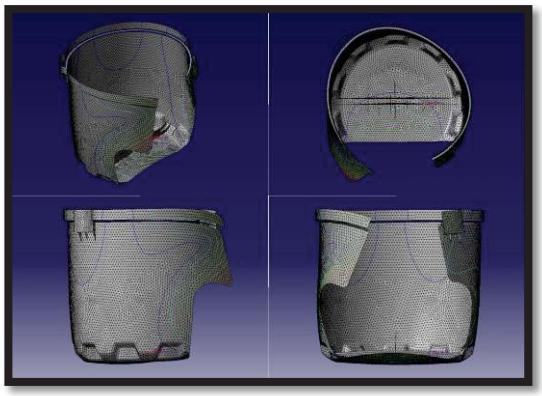	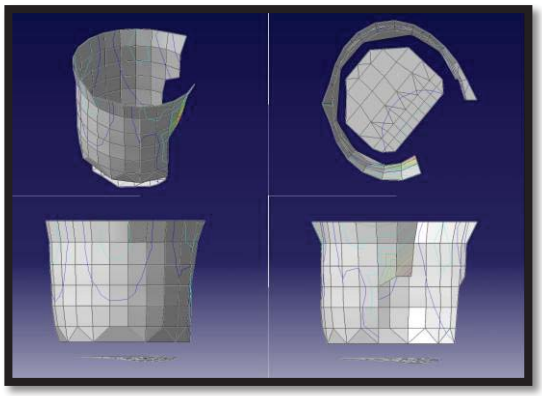
Analytical Modal Analysis ω_n=330.9 Hz	Experiment Modal Analysis ω_n=351.1 Hz ζ= 2.35%

Table 6.14: The sixth mode of the closed end cap. This mode shape shows the parts cross-section taking a partial triangular shape.

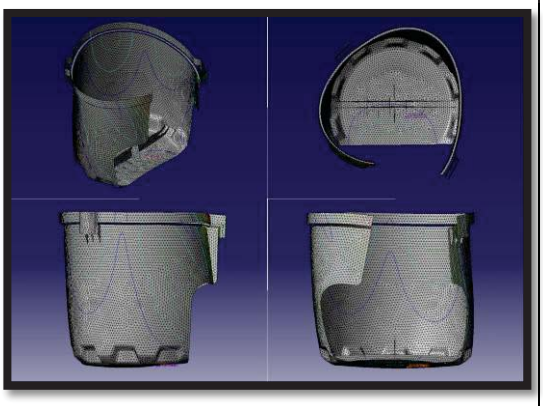	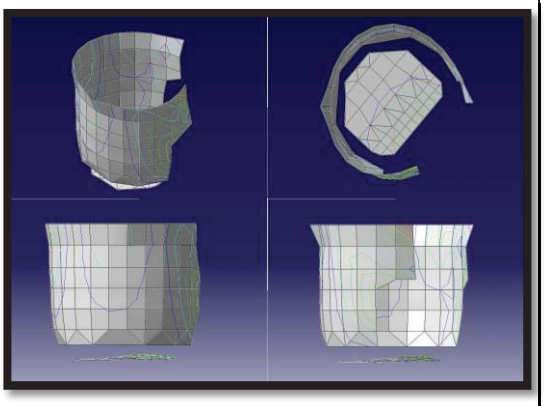
Analytical Modal Analysis ω_n=342.7 Hz	Experiment Modal Analysis ω_n=382.3 Hz ζ= 2.34%

Table 6.15: The seventh mode of the closed end cap. This mode shape shows the open end of the part rotating in the vertical plane.

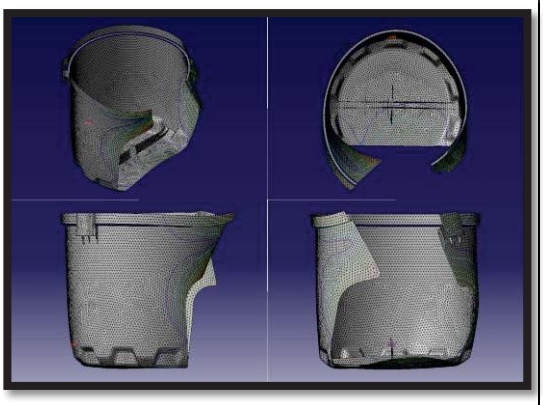	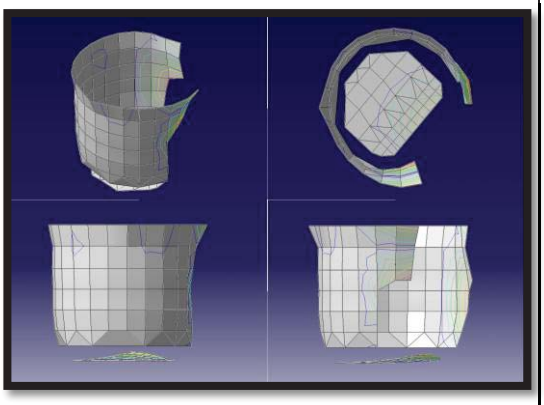
Analytical Modal Analysis ω_n=417.7 Hz	Experiment Modal Analysis ω_n=444.5 Hz ζ= 2.53%

Table 6.16: The eighth mode of the closed end cap. This mode shape shows the shell of the part bulging in and out, the top of the part is also showing a second order bending motion.

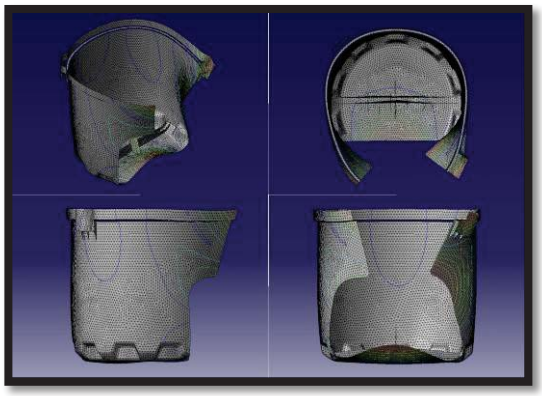	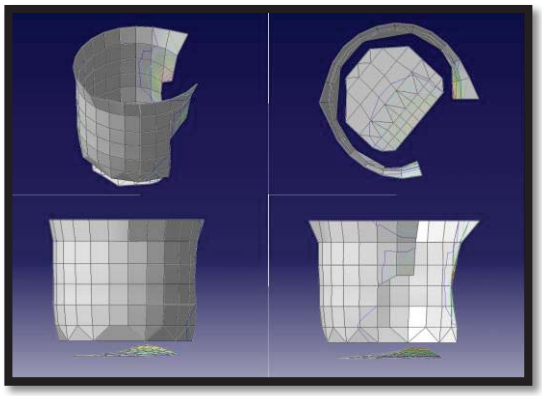
Analytical Modal Analysis ω_n=503.9 Hz	Experiment Modal Analysis ω_n=543.2 Hz ζ= 2.66%

Table 6.17: The ninth mode of the closed end cap. This mode shape shows the parts cross-section taking a partial triangular shape and the open end slightly flexing in and out.

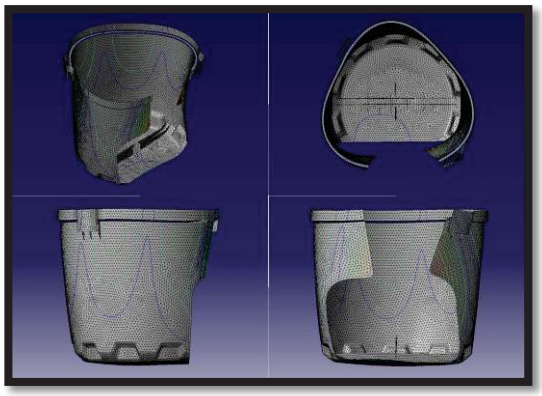	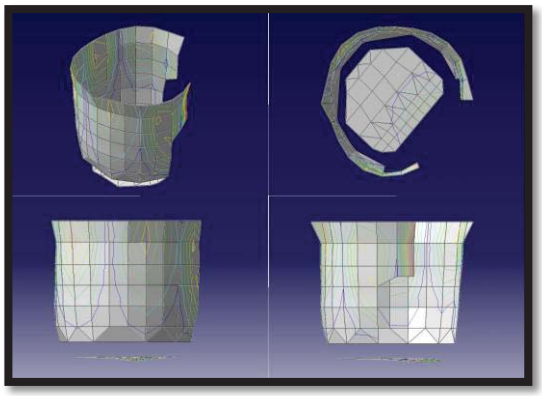
Analytical Modal Analysis ω_n=530.6 Hz	Experiment Modal Analysis ω_n=571.5 Hz ζ= 2.47%

Table 6.18: The tenth mode of the closed end cap. This mode shape shows the parts cross-section taking a square shape.

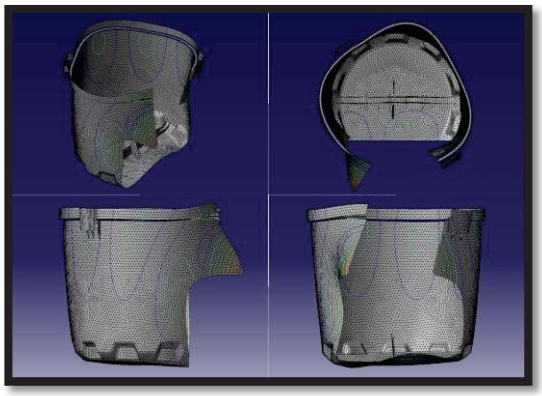	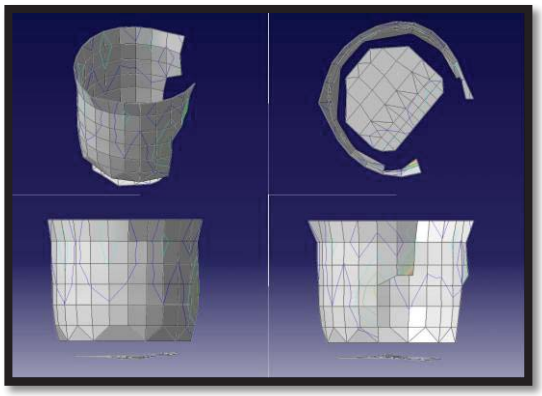
Analytical Modal Analysis ω_n=727.1 Hz	Experiment Modal Analysis ω_n=757.4 Hz ζ= 2.89%

Table 6.19: The Closed End Caps original mode pair table.

Test Mode ID	Frequency (Hz)	Finite Element Mode ID	Frequency (Hz)	MAC Value	Frequency Difference (Hz)	Frequency Difference (%)
1	63.7	7	63.1	0.979	0.63	1
2	98.1	8	91.8	0.881	6.27	6.4
3	112	9	104.7	0.652	7.27	6.5
4	202.5	10	194.1	0.979	8.36	4.1
5	351.1	11	330.9	0.870	20.19	5.8
6	382.3	12	342.7	0.852	39.63	10.4
7	444.5	13	417.7	0.925	26.84	6
8	543.2	14	503.9	0.852	39.25	7.2
9	571.5	15	530.6	0.620	40.86	7.1
10	757.4	16	727.1	0.907	30.31	4

After analysis of the mode shape images and mode pair table above it is concluded that the analytical and experimental modal analyses show a strong correlation. The evidence of this is indicated by the high MAC values, low frequency difference, and visual comparisons of the mode shape images. Only modes three and nine, shown above do not display a strong agreement. It is hypothesized that these discrepancies are due to degree of freedom differences between the mode shapes. This is because only radial motion was measured during the experimental modal analysis, where the FE model takes all six axes into

account. This type of error is taken account of in the MAC calculation but due to the specific shape, the degree of freedom reconciliation may not be possible.

The analytical model also predicts the natural frequencies well, with only one mode exceeding the target frequency difference of %10. Similar to the analysis of the open end cap, the reason for this difference is not absolutely understood, due the fact that there are several uncertainties in the FE model and test-analysis correlation. These uncertainties and differences will be accounted for in the model calibration.

6.1.3 The Center Sections Modal Analysis

Tables 6.20 and 6.21 show the results from the center sections analytical and experimental modal analysis. Several other mode shapes were found in the frequency range of interest but were omitted because they were not completely defined in the experimental data. This was because several of the mode shapes depict the shell having the same motion with the internal structures moving differently; this motion was not measured for the experimental modal analysis. Typically a pseudo-orthogonality check (Avitabile[2]) could be used to differentiate these mode shapes, but due to differences in the test and analysis mode shape vector coordinate systems as well as software limitations, this was not done. It was deemed that this is acceptable because the test and analysis mode shapes are very similar based on a visual inspection and the shapes in the frequency range of interest show acceptable MAC values. Because of this, the correlation confirms that the FE model accurately predicts the systems motion over the desired frequency range.

Table 6.20: First mode of the Center Section. This mode shows the shells cross section taking an oval shape, the rest of the part flexes to accommodate this motion.

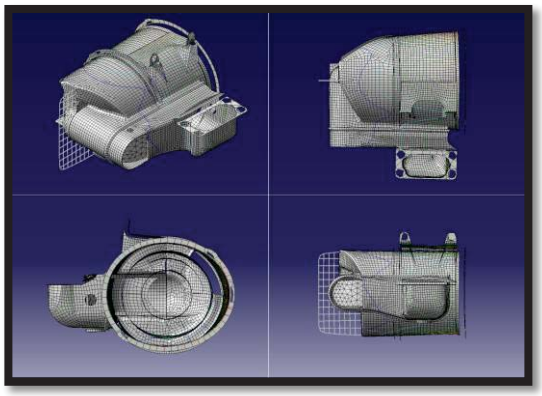	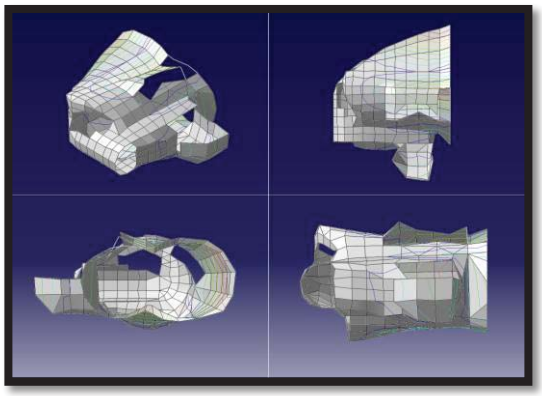
Analytical Modal Analysis ω_n=237.3 Hz	Experiment Modal Analysis ω_n=265.7 Hz ζ= 2.12%

Table 6.21: The second mode of the Center Section. This is a repeated mode shape of mode one, where the shape is slightly rotated.

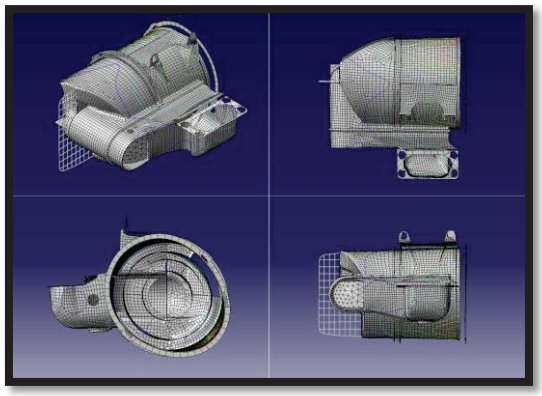	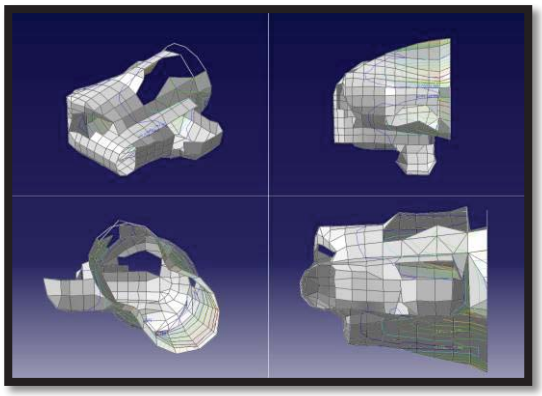
Analytical Modal Analysis ω_n=297.6 Hz	Experiment Modal Analysis ω_n=349.7 Hz ζ= 2.34%

Table 6.22: The Center Sections original mode pair table

Test Mode ID	Frequency (Hz)	Finite Element Mode ID	Frequency (Hz)	MAC Value	Frequency Difference (Hz)	Frequency Difference (%)
1	265.7	7	226.7	0.933	38.96	14.7
2	349.7	8	284.9	0.949	64.82	18.5

By observing the mode pair table it is seen that FE model under predicts the systems natural frequencies somewhat significantly. The FE model also under predicts the systems

mass; the parts mass based on the FE models properties is measured to be 536g while the mass of the physical part was measured to be 604g (~11.2% error). This under prediction in mass is assumed to be caused by the geometric simplifications and de-featuring. This is because the closed end of the center section is a complex shape, which is being approximated by flat surfaces. There are also several fillets, which have been remove as well that could lead to a large decrease in the systems mass. Attempts will be made to account for these errors during the model calibration.

6.2 Model Calibration

This section discusses the results from the model calibration; the focus in this section will be on the accuracy of the FE model's modal parameters. The calibrated model parameters and material properties (which are different for each FE model) are shown in chapter 9 appendix B. Table 6.23 shows the mode pair table for the open end caps calibrated FE model. As before, the first model check is the comparisons between the FE models and physical parts mass. The calibrated FE models mass is 188g (a 9% change from the original FE model). There is ~7% error in the in the global mass of the FE model. This is deemed to be acceptable, because as it is shown in the mode pair table, the FE model is still very predictive of the systems dynamics. Through comparisons between tables 6.23 and 6.8 it is seen that frequency difference is reduced to an acceptable level. It is also noticed that the MAC values between the test and analysis modes were also somewhat reduced as a result of the model calibration. While this an undesirable result, it is acceptable as the MAC values are still high and show a good correlation.

Table 6.23: The Open End Caps updated mode pair table

Test Mode ID	Frequency (Hz)	Finite Element Mode ID	Frequency (Hz)	MAC Value	Frequency Difference (Hz)	Frequency Difference (%)
1	265.2	7	249.5	0.846	15.76	5.9
2	274.3	8	251.9	0.839	22.41	8.2
3	714.9	9	679.4	0.648	35.54	5.0
4	724.8	10	684.3	0.637	40.57	5.6
5	844.2	13	933.8	0.989	89.66	10.6
6	1149.1	19	1182.8	0.929	33.73	2.9
7	1157.7	18	1176.2	0.919	18.50	1.6

Table 6.24 below shows the resulting mode pair table from the closed end caps model calibration. The calibrated FE models global mass is ~160g, the ~2.5% error between the FE model and the physical system is very small and is acceptable. Comparing tables 6.24 and 6.19 shows that the frequency difference goes up for some modes, while it goes down for others. This is acceptable because mean frequency error was decreased with the model calibration. Similar to the previous model calibration, the MAC values were slightly lowered. This is still considered acceptable as they still show a strong correlation.

Table 6.24: The Closed End Caps updated mode pair table

Test Mode ID	Frequency (Hz)	Finite Element Mode ID	Frequency (Hz)	MAC Value	Frequency Difference (Hz)	Frequency Difference (%)
1	63.7	7	64.7	0.979	1.01	1.6
2	98.1	8	94.2	0.863	3.89	4.0
3	112	9	107.6	0.632	4.37	3.9
4	202.5	10	200.4	0.978	2.10	1.0
5	351.1	11	339.3	0.813	11.78	3.4
6	382.3	12	352.9	0.774	29.45	7.7
7	444.5	13	428.5	0.922	16.01	3.6
8	543.2	14	516.9	0.868	26.22	4.8
9	571.5	15	547.1	0.652	24.39	4.3
10	757.4	16	748.7	0.905	8.75	1.2

Table 6.25 below, shows the center sections updated mode pair table. It should be noted that because of the unique goals of this model calibration (increase both the parts global mass and natural frequency values), it was performed manually by adjusting the material properties. This model calibration is deemed to be acceptable as the frequency difference was decreased and the systems global mass was increased to match the parts measured mass.

Table 6.25: The Center Sections updated mode pair table

Test Mode ID	Frequency (Hz)	Finite Element Mode ID	Frequency (Hz)	MAC Value	Frequency Difference (Hz)	Frequency Difference (%)
1	265.7	7	237.3	0.935	28.42	10.7
2	349.7	8	297.6	0.949	52.15	14.9

6.3 Assembled HDAC Modal Analysis

This section discusses the results from the assembled HDAC's modal analysis and model correlation. It is important to reiterate that the assembled FE model is constructed using connections, which are only rough approximation of the actual interfaces. This means that the modal parameters cannot be exactly defined using the FE model. Because of this, the expectations of the model correlation are much lower than they were for the components correlation. The results shown below are for both HDAC configurations (with and without the air filters) with the calibrated connection properties. Tables 6.26 through 6.29 show the corresponding mode shapes for the HDAC without the air filters, table 6.30 is the mode pair table for this configuration of the HDAC.

Table 6.26: The first mode of the assembled HDAC without the air filters. This mode shows the closed end cap swaying side to side.

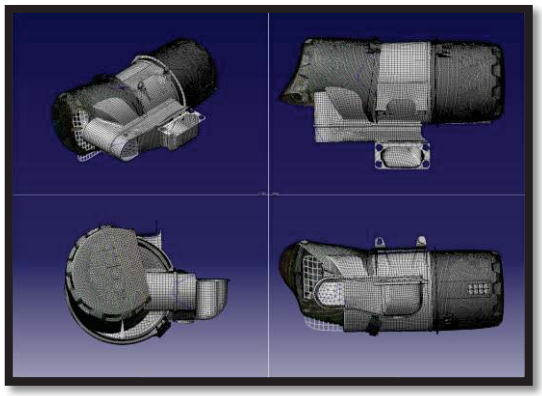	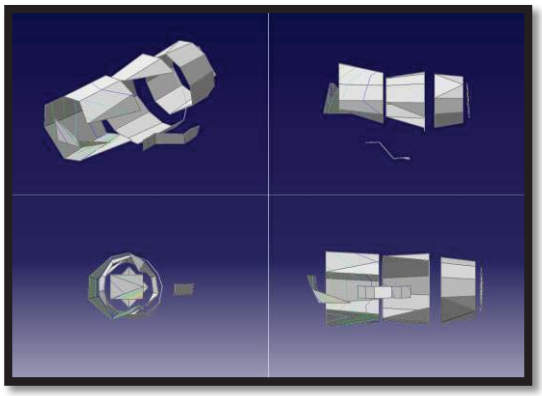
Analytical Modal Analysis ω_n=327.5 Hz	Experiment Modal Analysis ω_n=347.8 Hz

Table 6.27: The second mode of the assembled HDAC without the air filters. This mode shows the closed end cap swaying up and down

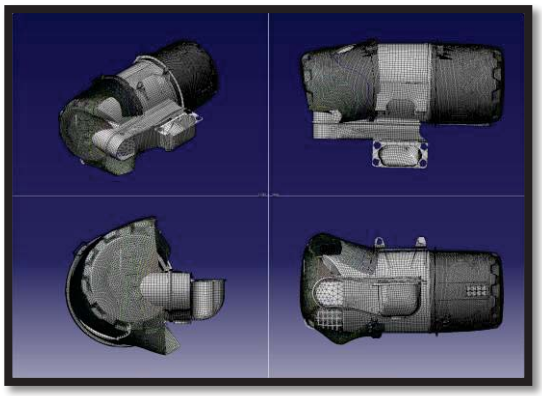	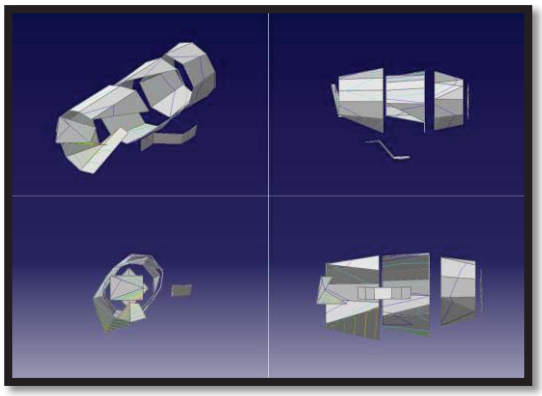
Analytical Modal Analysis ω_n=339 Hz	Experiment Modal Analysis ω_n=343.6 Hz

Table 6.28: The third mode of the assembled HDAC without the air filters. This mode shows the interface between the center section and the open end cap taking an oval shape.

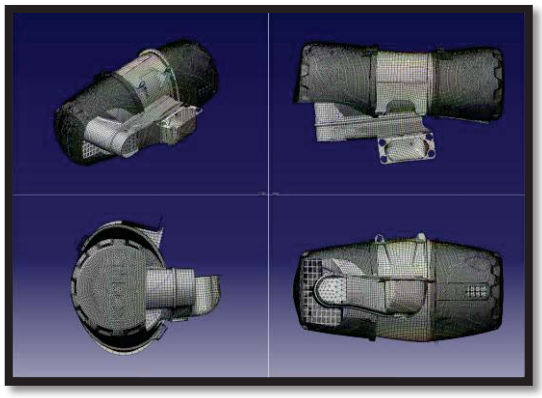

Analytical Modal Analysis
ω_n=366.9 Hz

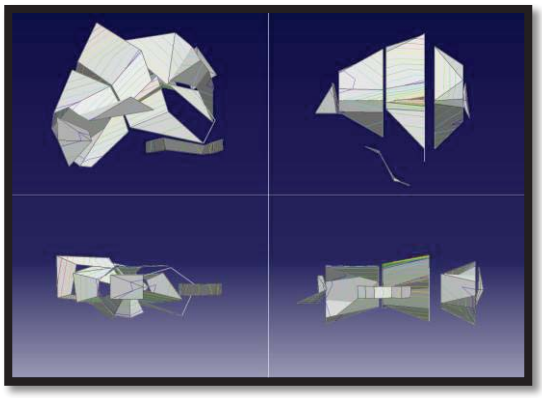

Experiment Modal Analysis
ω_n=361.1 Hz

Table 6.29: The fourth mode of the assembled HDAC without the air filters. This mode shows the interface between the center section and the open end cap taking an oval shape.

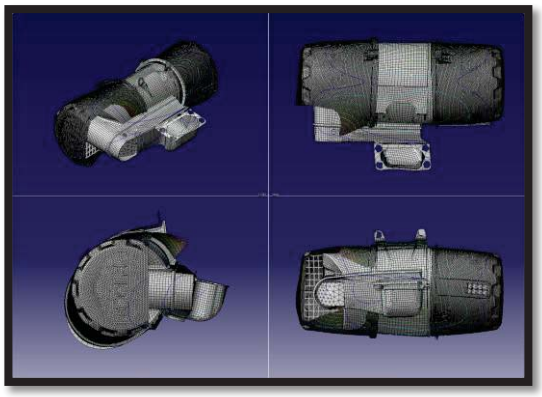

Analytical Modal Analysis
ω_n=420.2 Hz

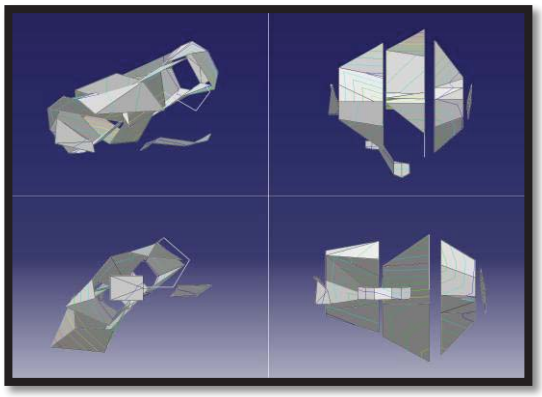

Experiment Modal Analysis
ω_n=396.8 Hz

Table 6.30: The mode pair table for the assembled HDAC without the air filters

Test Mode ID	Frequency (Hz)	Finite Element Mode ID	Frequency (Hz)	MAC Value	Frequency Difference (Hz)	Frequency Difference (%)
1	327.5	8	347.8	0.01	20.26	6.2
2	339	7	343.6	0.132	4.63	1.4
3	366.9	9	361.1	0.754	5.76	1.6
4	420.2	10	396.8	0.658	23.43	5.6

After reviewing the mode images and mode pair table above, confidence has been built in the FE models ability to predict the systems modal parameters. The third and fourth

modes correlate well, a visual comparison of the mode shapes shows strong evidence that the same mode shape is being portrayed. The first and second modes do not correlate as well. This was expected because it involves the interfaces between the closed end cap and the center section, which are nonlinear. It should also be noted that the first two mode shapes also exhibit complex motion, which isn't predicted by the FE model. After an in depth visual analysis of the mode shapes it is believed that the same mode shapes are being portrayed. Tables 6.31 through 6.34 show the corresponding mode shapes for the HDAC with the air filters and table 3.35 is the resulting mode pair table.

Table 6.31: The first mode of the assembled HDAC with the air filters. This mode shows the closed end cap swaying side to side.

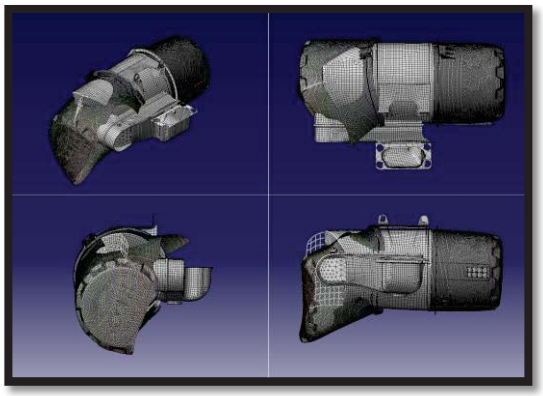	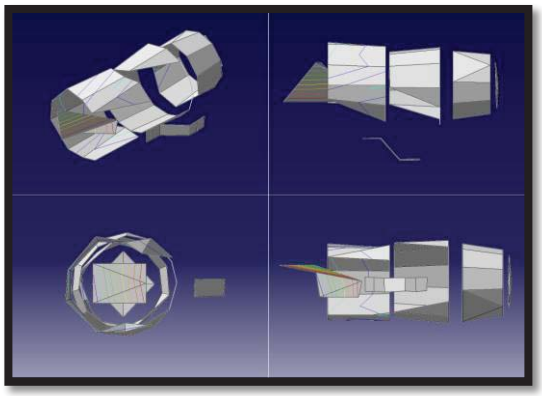
Analytical Modal Analysis ω_n=324.6 Hz	Experiment Modal Analysis ω_n=333.1 Hz

Table 6.32: The second mode of the assembled HDAC with the air filters. This mode shows the closed end cap swaying up and down

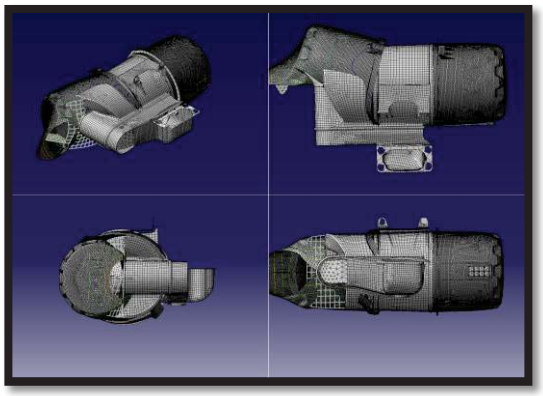	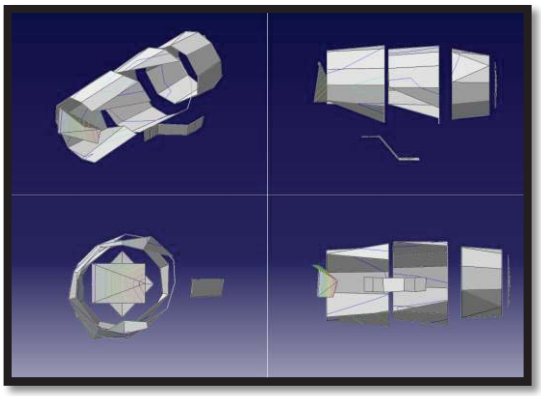
Analytical Modal Analysis ω_n=338.2 Hz	Experiment Modal Analysis ω_n=327 Hz

Table 6.33: The third mode of the assembled HDAC with the air filters. This mode shows the interface between the center section and the open end cap taking an oval shape.

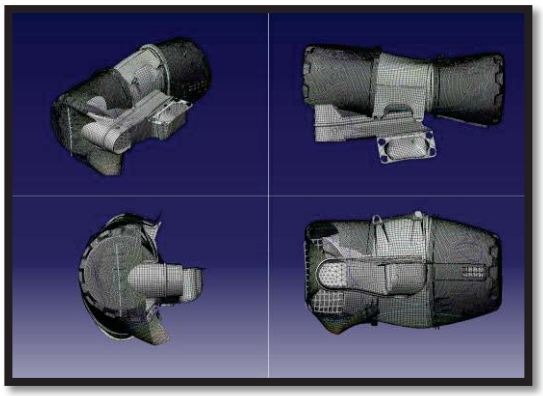	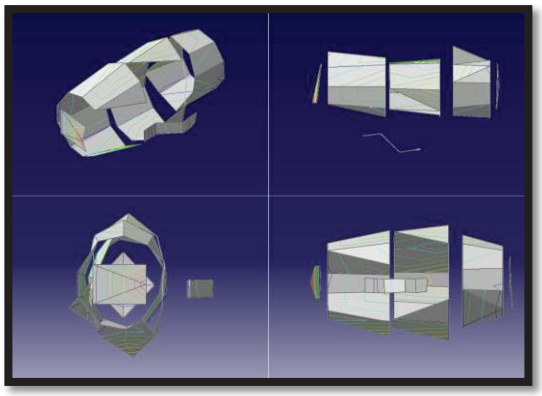
Analytical Modal Analysis ω_n=343.3 Hz	Experiment Modal Analysis ω_n=409.9 Hz

Table 6.34: The fourth mode of the assembled HDAC with the air filters. This mode shows the interface between the center section and the open end cap taking an oval shape.

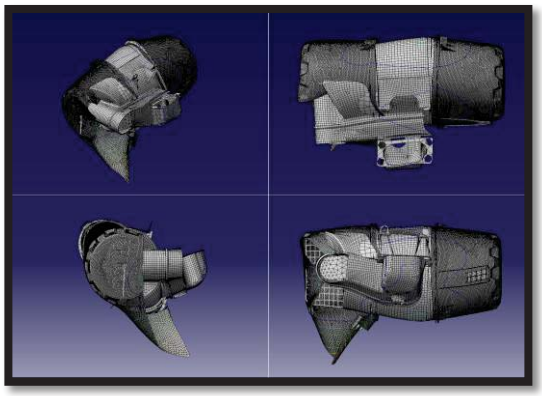	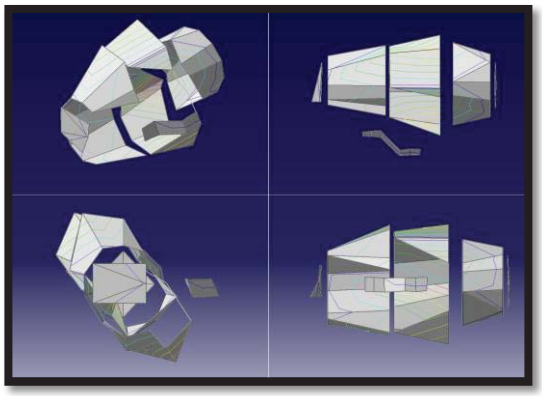
Analytical Modal Analysis ω_n=411.8 Hz	Experiment Modal Analysis ω_n=429.6 Hz

Table 6.35: The mode pair table for the assembled HDAC with the air filters

Test Mode ID	Frequency (Hz)	Finite Element Mode ID	Frequency (Hz)	MAC Value	Frequency Difference (Hz)	Frequency Difference (%)
1	324.6	12	333.1	0.088	8.55	2.6
2	338.2	11	327	0.064	11.15	3.3
3	343.3	15	409.9	0.462	66.6	19.4
4	411.8	16	429.6	0.715	17.72	4.3

The results for this configurations modal analysis and model correlation are very similar to the results for configuration without the air filters. This is expected since it is assumed that the air filters only effect the system because of their added mass. The mode shapes don't correlate as well for this configuration as they did for the configuration without the air filters. Again, this makes sense because the air filters add significant uncertainty to the FE model. Based on a visual inspection and the evidence in the mode pair table it is concluded that both models are predicting the same mode shapes.

6.4 Dynamic Response Prediction and Measurement

Figures 6.1 through 6.4 below show the measured and predicted responses for the assembled HDAC with and without the air filters. As a reminder, the simple input spectrum

was used to calibrate the FE models damping properties and the complex input spectrum was used for blind prediction. Tables 6.36 through 6.38 below show the overall RMS levels for all of the systems responses. These tables also show the differences in the overall level between the measured and predicted responses.

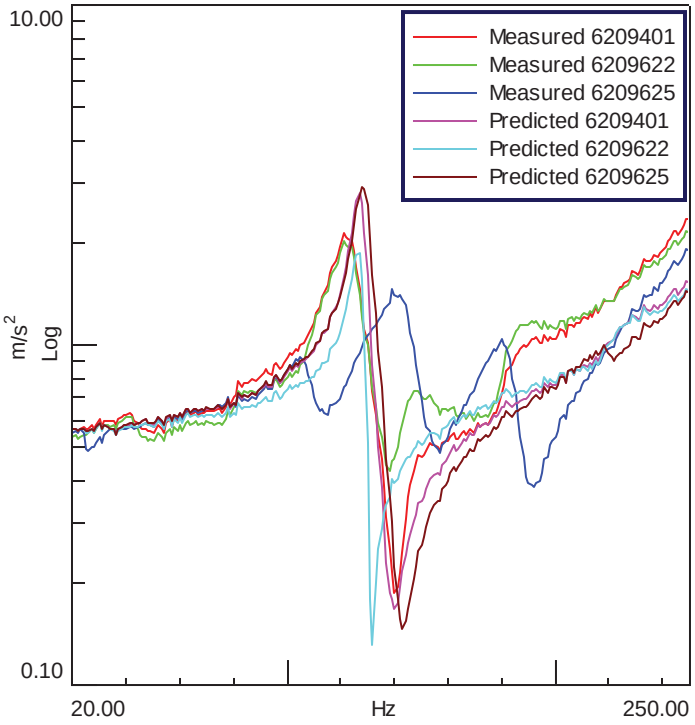

Figure 6.1: The dynamic response of the assembled HDAC without the air filters due to the simple input spectrum.

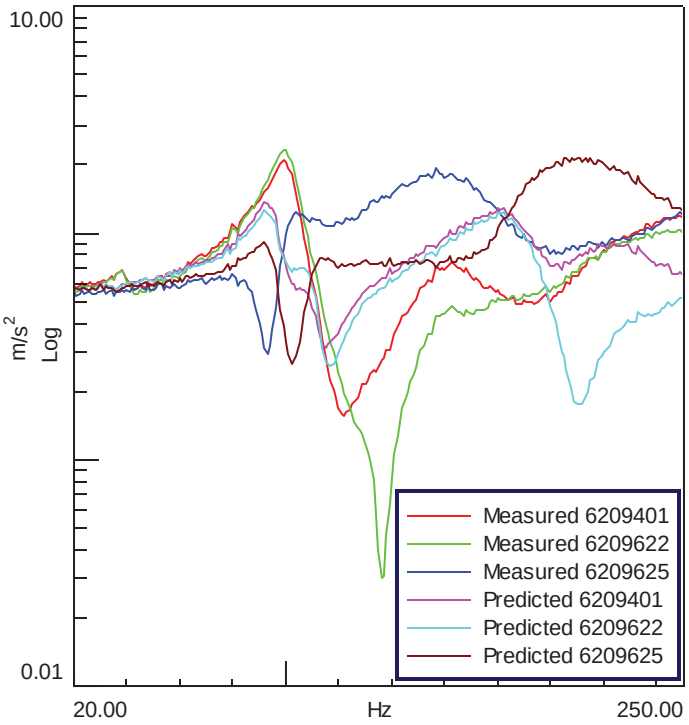

Figure 6.2: The dynamic response of the assembled HDAC with the air filters due to the simple input spectrum.

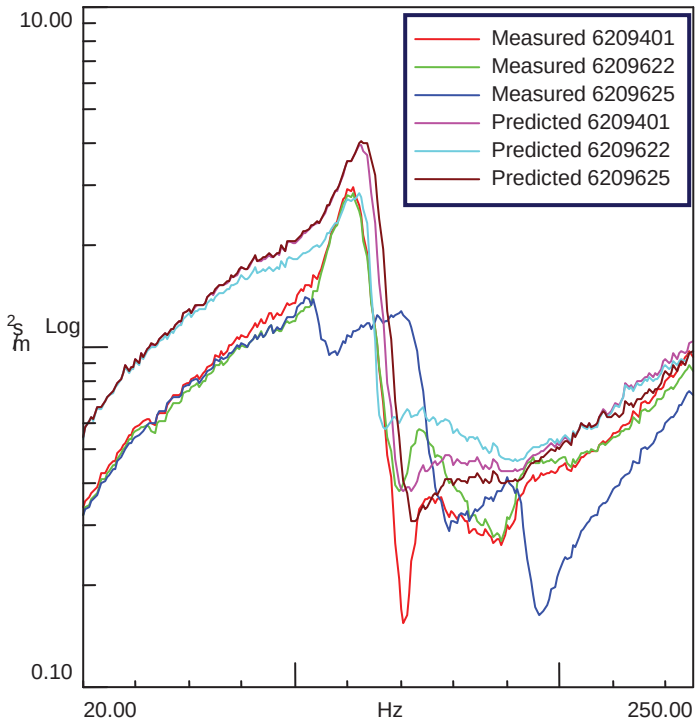

Figure 6.3: The dynamic response of the assembled HDAC without the air filters due to the complex input spectrum.

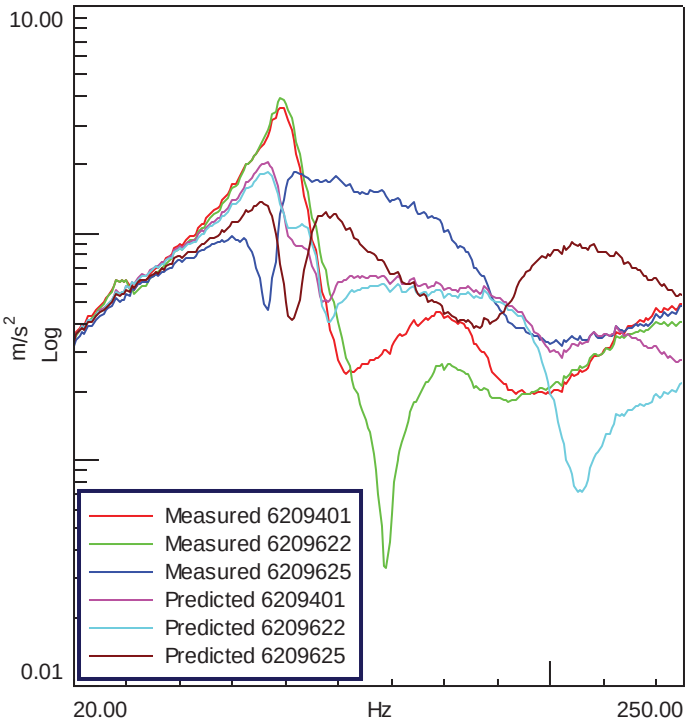

Figure 6.4: The dynamic response of the assembled HDAC with the air filters due to the complex input spectrum.

Table 6.36: Assembled HDAC overall RMS response level for the measurement point on the closed end cap (dB reference = 1 m/s^2)

Input Spectrum	HDAC Assembly with Filter (dB)			HDAC Assembly without Filter (dB)		
	Measured	Predicted	Difference	Measured	Predicted	Difference
Simple	25.42	25.89	-0.47	23.74	24.10	-0.36
Complex	24.35	22.61	1.74	22.55	23.89	-1.34

Table 6.37: Assembled HDAC overall RMS response level for the measurement point on the open end cap (dB reference = 1 m/s^2)

Input Spectrum	HDAC Assembly with Filter (dB)			HDAC Assembly without Filter (dB)		
	Measured	Predicted	Difference	Measured	Predicted	Difference
Simple	23.16	21.93	1.23	25.31	23.10	2.21
Complex	25.43	22.15	3.28	24.41	22.20	2.21

Table 6.38: Assembled HDAC overall RMS response level for the measurement point on the center section (dB reference = 1 m/s^2)

Input Spectrum	HDAC Assembly with Filter (dB)			HDAC Assembly without Filter (dB)		
	Measured	Predicted	Difference	Measured	Predicted	Difference
Simple	23.22	23.09	0.13	25.41	24.04	1.37
Complex	25.05	22.63	2.42	24.76	23.63	1.13

The figures and tables above show that the FE model predicts responses, which come very close to meeting the goals of the project. The predicted spectrums for the points on the open end cap and the center section resemble the same shape as the measured spectrums; especially for assembly without the air filters. The closed end caps predicted spectrums do not match the measured responses quite as closely; although they do resemble the same shape (except for the case with the simple input spectrum without the air filters). As with the modal analysis this error is assumed to be caused by the non-linear interfaces between the closed end cap and the center section.

The FE models predicted overall RMS levels match the measured results closely, with only one measurement point (on the open end cap with the air filters in the assembly) that does not meet the goals of the project. This one point is not far off the goal of +/- 3 dB of error, with the predicted level being 3.28 dB higher then the measured response meaning that it is still considered to be an accurate result. Again, the reason for this error is assumed to be caused by the uncertainty in the connections between the closed end cap and the center section.

It is interesting to note that while the predicted spectrums for the measurement point on the closed end cap more closely represents the shape of the measured response, there is more error in the predicted overall level. This error is most likely caused by incorrect air filter damping properties, either in the connections or the air filters FE model. This is because the FE models damping matrix is calculated using a single structural damping coefficient. It makes sense that this would cause issues since the air filters material properties are most likely significantly different from the plastic components. As such, using the same damping coefficient for both of them would most likely cause some modeling error.

Chapter 7: Conclusions

The work in this thesis presents a finite element model, which has been shown to be useful to predict the dynamic response of a Kohler Engines Heavy Duty Air Cleaner. The FE models accuracy has been demonstrated at both the component and assembly level. This was done through comparisons between the analytical and experimental modal parameters as well as comparisons between measured and predicted dynamic responses.

To create this FE model, the individual components of the HDAC were analyzed. Through this it was found that the parts could be accurately modeled using one and two dimensional finite elements. Concurrently, it was found that a roving impact hammer modal test could be used to collect the parts experimental modal data. The component FE models accuracy was verified using model correlation techniques to ensure that they predict the physical systems modal properties. Once confidence was built in the FE models predictive capabilities their accuracy was improved through the calibration of various model parameters.

It was found that the different component interfaces could be approximated using bush connection properties to model the connections with relative accuracy. The HADC's FE model was assembled in two different configurations, with and without the air filters. The connections stiffness and damping properties were determined using two different sets of experimental data. The connection stiffness's were found using comparisons to experimental modal data, while the connections damping properties were found using comparisons to the systems measured response due to a simple input.

The assembled models predictive capability was checked using a blind prediction of the systems dynamic response to a broadband random input. It was found that the predicted

responses portray the same general shape as the measured responses. It was also found that the FE model could accurately predict the overall level of the response, with the worst prediction being 3.28 dB greater then measured RMS response level.

7.1 Recommendations for Future Work

There are several areas where this project could be improved and expanded upon in future work. This thesis focused on the HDAC in a quasi-linear state and making an FE model, which was simple and straightforward to apply. It is suggested that in the future more sophisticated techniques are used better understand the system. This includes nonlinear analytical and experimental modal analyses to better define the systems modal properties. As well as applying more sophisticated connection modeling techniques. It is suspected that the errors in the response predictions are caused by the approximated connections. If this is true, the models accuracy could be increased by improving these connections.

It is also suggested that a model validation be performed to verify the models accuracy. This validation experiment could include the use of a more sophisticated and realistic input profile. In addition to this, more test samples should be tested and compared to the model to create statistical confidence in the validation experiments results.

Chapter 8: References

1. Hasselman Timothy K., Coppolino Robert N., Zimmerman David C. Criteria for Modeling Accuracy: A State-of-the-Practice Survey. Proceedings of the International Modal Analysis Conference. 2000;1:335-341.
2. Avitabile Peter, O'Callahan John, Milani John. Model Correlation and Orthogonality Criteria. Proceedings of the International Modal Analysis Conference. 1988;1:1039-1047.
3. Allemang Randall J. The Modal Assurance Criteriaon (MAC): Twenty Years of Use and Abuse. Proceedings of the International Modal Analysis Conference. 2002;1:397-405.
4. Heylen Ward, Lammens Stefan, Sas Paul. Modal Analysis Theory and Testing. 2nd. Belgium: Katholiekee Universiteit Leuven; 1998.
5. Flanigan Christopher C. Model Reduction Using Guyan, IRS, and Dynamic Methods. Proceedings of the International Modal Analysis Conference. 1998:1:172-176.
6. Guyan Robert J. Reduction of Stiffness and Mass Matrices. AIAA Journal. 1965;3(2):380.
7. O'Callahan John, Avitabile Peter. System Equivalent Reduction Expansion Process (SEREP). Proceedings of the 7th International Modal Analysis Conference. 1989;1:29-37.
8. Avitabile Peter. Correlation Considerations – Part 3 (Experimental Modal Testing Considerations for Finite Element Model Correlation). Proceedings of the International Modal Analysis Conference. 1998;1:185-196.

9. Blaschke Peter, Mueller-Held Bernhard. Identification of Dynamic Young's Modulus and Damping of Isotropic Plastic Materials. Proceedings of the 27th International Modal Analysis Conference. 2009;1.
10. Veers Paul S, Laird Daniel L, Carne Thomas G, Sagartz Mathias J. Estimation of Uncertain Material Parameters Using Modal Test Data. AIAA Aerospace Sciences Mtg. / ASME Wind Energy Symposium. 1998;19:1-11.
11. Smith Steven W. Digital Signal Processing: A Practical Guide for Engineers and Scientists. 1st . Newnes, 2003
12. Mayes Randy L. Model Correlation and Calibration. Proceedings of the 27th International Modal Analysis Conference. 2009;1.

Chapter 9: Appendices

9.1 Appendix A – Data Acquisition Set-Up

Table 9.1: The Open End Caps modal test data acquisition parameters

Sampling Rate	Frequency Resolution	Number of Averages	Averaging Type	Response Window	Reference Window	FRF Estimator Type
3200Hz	0.195Hz	10	Linear	Uniform	Uniform	H1

Table 9.2: The Closed End Caps modal test data acquisition parameters

Sampling Rate	Frequency Resolution	Number of Averages	Averaging Type	Response Window	Reference Window	FRF Estimator Type
1638.4Hz	0.2Hz	5	Linear	Uniform	Force Exponential	H1

Table 9.3: The Center Sections modal test data acquisition parameters

Sampling Rate	Frequency Resolution	Number of Averages	Averaging Type	Response Window	Reference Window	FRF Estimator Type
3276.8Hz	0.8Hz	10	Linear	Uniform	Force Exponential	H1

Table 9.4: HDAC assembly modal test data acquisition parameters

Sampling Rate	Frequency Resolution	Number of Averages	Averaging Type	Response Window	Reference Window	FRF Estimator Type
1280Hz	0.625Hz	10	Linear	Uniform	Uniform	H1

Table 9.5: HDAC assembly shaker test data acquisition parameters

Sampling Rate	Frequency Resolution	Number of Averages	Averaging Type	Response Window
800Hz	1Hz	~100	Linear	Hanning

9.2 Appendix B – Component FE Model Set-Up

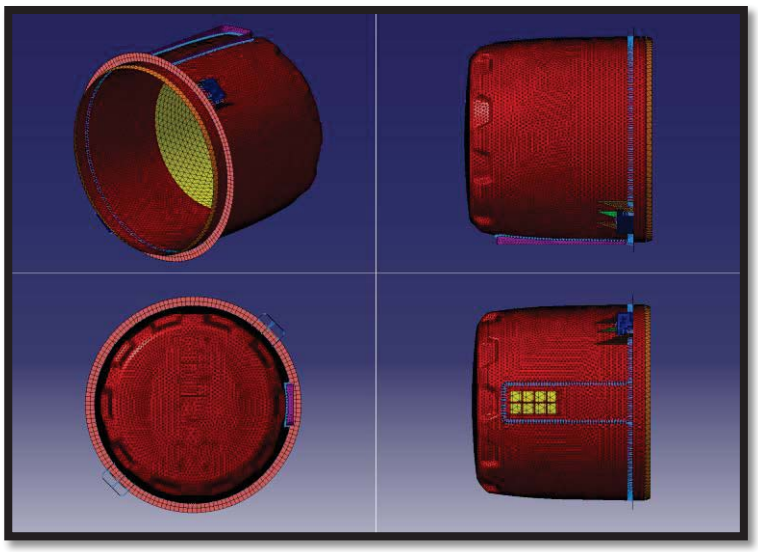

Figure 9.1: Image showing the different mesh domains of the Open End Caps FE model.

Table 9.6: The Open End Caps FE model mesh domain properties.

Property ID	1	2	3	4	5	6	7	8
Color	Yellow	Orange	Red	Pink	Purple	Blue	Brown	Green
Mesh Thickness (mm)	1	1mm	2.5	3	2.009	2.218	1.77	2.022
Updated Mesh Thickness (mm)	0.995	1.002	2.513	3.3	2.02	2.21mm	1.779	2.019

Table 9.7: The Open End Caps material properties.

Property	Default Material Properties	Calibrated Material Properties
Youngs Modulus (N/m^2)	3442×10^6	3792×10^6
Poissons Ratio	.3	.2727
Density (Kg/m^3)	1040	936

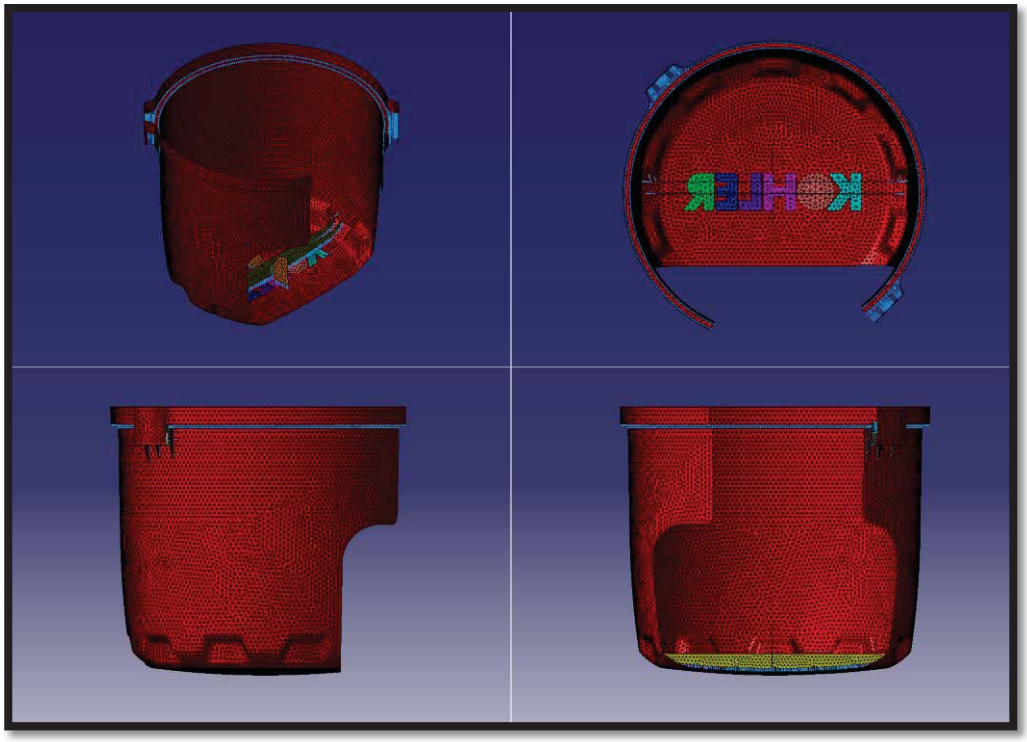

Figure 9.2: Image showing the different mesh domains of the Closed End Caps FE model.

Table 9.8: The Closed End Caps FE model mesh domain properties.

Property ID	Color	Mesh Thickness (mm)	Calibrated Mesh Thickness (mm)
1	Yellow	1.833	1.836
2	Orange	3.009	3.007
3	Red	2.5	2.551
4	Pink	2.086	2.086
5	Purple	1.503	1.503
6	Lavender	1.56	1.56
7	Blue	2.019	2.019
8	Light Blue	3.433	3.434
9	Light Green	3.433	3.434
10	Dark Green	2.1	2.1
11	Tan	2.074	2.073
12	Brown	1.77	1.77
13	Black	2.022	2.022

Table 9.9: The Closed End Caps material properties.

Property	Default Material Properties	Calibrated Material Properties
Youngs Modulus (N/m^2)	3442×10^6	3546×10^6
Poissons Ratio	.3	.3144
Density (Kg/m^3)	1040	1040

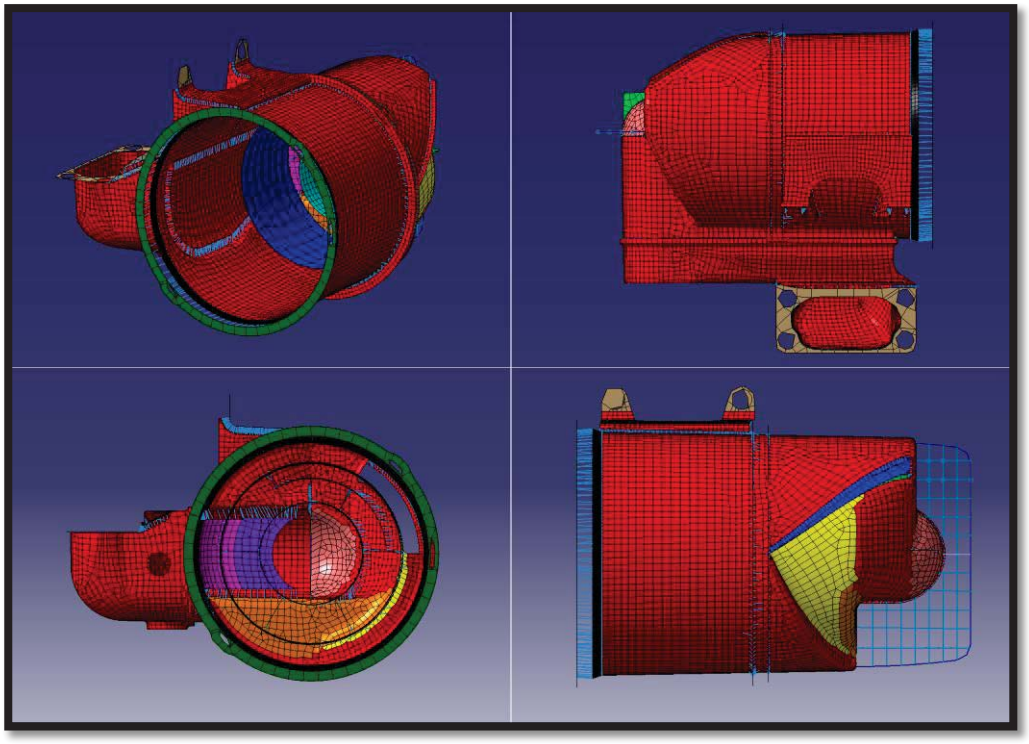

Figure 9.3: Image showing the different mesh domains of the Center Sections FE model.

Table 9.10: The Center Sections FE model shell element mesh domain properties.

Property ID	Color	Mesh Thickness (mm)
1	Red	3
2	Yellow	3.442
3	Orange	2.6
4	Pink	4.594
5	Purple	0.615
6	Lavender	3.362
7	Blue	1.668
8	Light Blue	1.513
9	Light Green	4.01
10	Dark Green	9
11	Tan	8
12	Brown	2
13	Dark Red	3.518
14	Black	1.588
15	White	2.939

Table 9.11: The Center Sections FE model shell element mesh domain properties.

Property	Area (m^2)	I_{yy}(m^4)	I_{zz}(m^4)	J (m^2)
Bar1	1.5×10^{-5}	3.125×10^{-11}	1.125×10^{-11}	2.817×10^{-11}
Beam1	7.5×10^{-6}	1.406×10^{-11}	1.562×10^{-11}	4.563×10^{-11}
Beam2	1.75×10^{-5}	1.786×10^{-11}	3.646×10^{-11}	4.057×10^{-11}

Table 9.12: The Center Sections material properties.

Property	Default Material Properties	Calibrated Material Properties
Youngs Modulus (N/m^2)	3442×10^6	4200×10^6
Poissons Ratio	.3	.3144
Density (Kg/m^3)	1040	1175

9.3 Appendix C – Component Connection Parameters

Table 9.13: Connection properties for the interface between the Open End cap and the Center Sections shell.

Connection Stiffness					
X-X	55000 N/m	Y-Y	65000 N/m	Z-Z	65000 N/m
RX-RX	150000 N·m/rad	RY-RY	150000 N·m/rad	RZ-RZ	150000 N·m/rad
Connection Viscous Damping Coefficients					
X-X	0.05 Kg/s	Y-Y	0.05 Kg/s	Z-Z	0.05 Kg/s
RX-RX	0.05 m^2·Kg/s ·rad	RY-RY	0.05 m^2·Kg/s ·rad	RZ-RZ	0.05 m^2·Kg/s ·rad

Table 9.14: Connection properties for the interface between the Open End cap and the air filters.

Connection Stiffness					
X-X	100 N/m	Y-Y	100 N/m	Z-Z	100 N/m
RX-RX	100 N·m/rad	RY-RY	100 N·m/rad	RZ-RZ	100 N·m/rad
Connection Viscous Damping Coefficients					
X-X	0.225 Kg/s	Y-Y	0.225 Kg/s	Z-Z	0.225 Kg/s
RX-RX	0.4 m^2·Kg/s ·rad	RY-RY	0.4 m^2·Kg/s ·rad	RZ-RZ	0.4 m^2·Kg/s ·rad

Table 9.15: Connection properties for the interface between the Closed End Cap and the Center Sections shell.

Connection Stiffness					
X-X	8000 N/m	Y-Y	8000 N/m	Z-Z	8800 N/m
RX-RX	35000 N·m/rad	RY-RY	33000 N·m/rad	RZ-RZ	28000 N·m/rad
Connection Viscous Damping Coefficients					
X-X	0.02 Kg/s	Y-Y	0.02 Kg/s	Z-Z	0.02 Kg/s
RX-RX	0.02 m^2·Kg/s ·rad	RY-RY	0.02 m^2·Kg/s ·rad	RZ-RZ	0.02 m^2·Kg/s ·rad

Table 9.16: Connection properties for the interface between the Closed End Cap and the Center Sections mesh grid.

Connection Stiffness					
X-X	7000 N/m	Y-Y	7000 N/m	Z-Z	9000 N/m
RX-RX	25000 N·m/rad	RY-RY	25000 N·m/rad	RZ-RZ	25000 N·m/rad
Connection Viscous Damping Coefficients					
X-X	0.1 Kg/s	Y-Y	0.1 Kg/s	Z-Z	0.1 Kg/s
RX-RX	0.1 m^2·Kg/s ·rad	RY-RY	0.1 m^2·Kg/s ·rad	RZ-RZ	0.1 m^2·Kg/s ·rad

Table 9.17: Connection properties for the interface between the Center Section and the air filters.

Connection Stiffness					
X-X	2500 N/m	Y-Y	2500 N/m	Z-Z	2500 N/m
RX-RX	2500 N·m/rad	RY-RY	2500 N·m/rad	RZ-RZ	2500 N·m/rad
Connection Viscous Damping Coefficients					
X-X	0.225 Kg/s	Y-Y	0.225 Kg/s	Z-Z	0.225 Kg/s
RX-RX	0.4 m^2·Kg/s ·rad	RY-RY	0.4 m^2·Kg/s ·rad	RZ-RZ	0.4 m^2·Kg/s ·rad

9.4 Appendix D – Filter FE Model Set-Up

Table 9.18: The air filters FE model shell element mesh domain properties.

Property	Area (m^2)	I_{yy}(m^4)	I_{zz}(m^4)	J (m^2)
Tube Type Beam	0.026	8.118×10^{-5}	8.118×10^{-5}	1.624

Table 9.19: The air filter FE model material properties.

Property	Estimated Material Properties
Youngs Modulus (N/m^2)	2.5×10^6
Poissons Ratio	.3
Density (Kg/m^3)	70.8